CD1d is an MHC-like glycoprotein that presents lipid antigen to natural killer T (NKT) cells (8–10). In humans, a specific subset of NKT cells expresses an invariant Vα24-JαQ/Vβ11 T cell receptor and can recognize CD1d on the surface of antigen presenting cells through this receptor (9). Like MHC class I HC, CD1d HC is synthesized, glycosylated by *N*-glycosyltransferase, modified, and assembled with β2m within the endoplasmic reticulum (ER) (10–12). Unlike MHC class I HC, CD1d HC is not affected by quality control mechanisms that efficiently destroy misfolded *N*-linked membrane glycoproteins and those that have not properly assembled with β2m (10, 11, 13). In fact, diverse CD1d HC isoforms, including mature glycosylated (~48 kDa), immature glycosylated (~45 kDa), and non-glycosylated (~37 kDa) forms, are expressed on the cell surface in a cell-type specific fashion (10–12).

CD1d plays a role in both innate and adaptive immunity to various bacteria, viruses, fungi, and parasites (14, 15). Activation of CD1d-restricted invariant NKT cells enhances host resistance to these microbes. CD1d-restricted NKT cells can act directly on infected cells, killing the CD1d-expressing cell. They also promote interferon γ production by conventional NK cells and modulate adaptive immune cells by altering Th1/Th2 polarization. Recognition of CD1d by invariant NKT cells causes rapid release of interleukin-4 and interferon γ from the NKT cell (9). The activation of CD1d-restricted invariant NKT cells in response to microbial invasion is antigen-dependent, but these antigens can be derived from the invading microbe or possibly host antigens (16–18).

Viewing the importance of CD1d in innate immune responses to microbes, we hypothesized that *C. trachomatis* may alter CD1d-mediated immune pathways and thereby avoid innate immune destruction of the infected cell by the host. Here we demonstrate that surface-expressed CD1d in human urethral epithelial cells is down-regulated by *C. trachomatis* infection, and this involves both CPAF-mediated and classic cytosolic proteasomal pathways.

MATERIALS AND METHODS

Epithelial Cell Line—The PURL epithelial cell line was established from penile urethra collected at autopsy under IRB approval. Small pieces of tissue were cultured in supplemented keratinocyte growth media (Invitrogen) and 0.4 mM calcium until epithelial outgrowth occurred. Primary cells were transduced with a retroviral vector (LXSN-16E6E7) (22), selected by resistance to the neomycin analogue G418 and passaged over 20 times prior to experiments. The cytokeratin profile (positive for CK13, -17, and -18), and the expression of the secretory component of the polymeric immunoglobulin receptor (SC) confirmed derivation from penile urethral epithelium.

C. trachomatis Infection—Near confluent PURL cells were overlaid with *C. trachomatis* serovar F (strain F/IC-Cal-13) elementary bodies suspended in a sucrose-phosphate-glutamate solution at a predetermined dilution that resulted in 80–85% of cells becoming infected. Plates were centrifuged for 1 h, supernatants were aspirated after centrifugation, and cells cultured for up to 45 h at 37 °C in keratinocyte growth media.

Antibodies—For anti-CD1d antibodies, a D5 mAb (mIgG2b (11)) recognizing all isoforms of CD1d HC was used for biochemical experiments. An NOR3.2 mAb (mIgG1, Abcam Inc., Cambridge, MA) recognizing all isoforms was used for flow cytometry and immunofluorescence. A 51.1.3 mAb (mIgG2b (10)) recognizing only mature glycosylated-CD1d was used for immunofluorescence. For anti-CPAF antibodies, an n54b mAb (mIgG1 (6)) recognizing N terminus and a c100a mAb (mIgG1 (7)) recognizing C terminus fragments of CPAF (kind gifts from Dr. G. Zhong, University of Texas, San Antonio, TX) were used for immunoprecipitation and immunoblotting, respectively. The n54b mAb was also used for immunofluorescence.

Flow Cytometry—PURL cells infected with *C. trachomatis* were harvested 24 h after infection. Uninfected and infected PURL cells were harvested using accutase (Chemicon, Temecula, CA). Harvested cells were then incubated with an anti-transferrin receptor mAb conjugated to phycoerythrin (Caltag Laboratories) or with an anti-CD1d NOR3.2 mAb for 30 min at 4 °C. CD1d staining was followed by a goat anti-mouse Ig secondary antibody conjugated to phycoerythrin for 30 min at 4 °C (BD Biosciences, San Jose, CA). Cells were suspended in 1% paraformaldehyde and analyzed using a FACSCalibur flow cytometry system (BD Biosciences).

Proteasome Inhibitor Treatment—Infected and control PURL cells were cultured for up to 45 h in the presence or absence of two different cytosolic proteasome inhibitors: lactacystin (2 or 10 μM) or MG132 (2 or 10 μM, Sigma-Aldrich) in Me_2SO. Control wells included vehicle alone.

Immunoprecipitation and Western Immunoblotting—Harvested PURL cells were lysed in modified radioimmune precipitation assay buffer (1% Nonidet P-40, 1% deoxycholate, 0.1% SDS, 10 mM Tris, 150 mM NaCl, 2 mM EDTA) with protease inhibitors (Amersham Biosciences). Equivalent aliquots of cell lysates were incubated overnight at 4 °C with 5 μg/ml of anti-CD1d D5 mAb or anti-CPAF n54b and 5 μl of Protein-A-Sepharose (Amersham Biosciences). Precipitated proteins were separated by SDS-PAGE using 8 or 10% acrylamide gels and transferred to polyvinylidene difluoride membranes. Purified CPAF c-fragment proteins (a kind gift from Dr. G. Zhong, University of Texas, San Antonio, TX) were included as positive controls. Anti-CD1d D5 mAb, anti-CPAF c100a mAb, or a rabbit anti-β-actin polyclonal antibody (Abcam Inc.) were used as primary reagents for immunoblotting and peroxidase-conjugated goat anti-mouse or anti-rabbit IgG antibodies (Pierce) as secondary reagents. A peroxidase-conjugated mouse anti-ubiquitin antibody (P4D1, Santa Cruz Biotechnology, Santa Cruz, CA) was used to detect ubiquitin. Products in Western immunoblotting experiments were visualized using standard chemiluminescence (Amersham Biosciences). Molecular weights were confirmed by comparison to standard size markers and molecular weight analysis (FluorChem™SP, Alpha Innotech, San Leandro, CA).

Endoglycosidase-H Treatment—D5-precipitated CD1d HCs were denatured and incubated overnight at 37 °C with endoglycosidase-H (New England Biolabs, Beverly, MA) in reaction

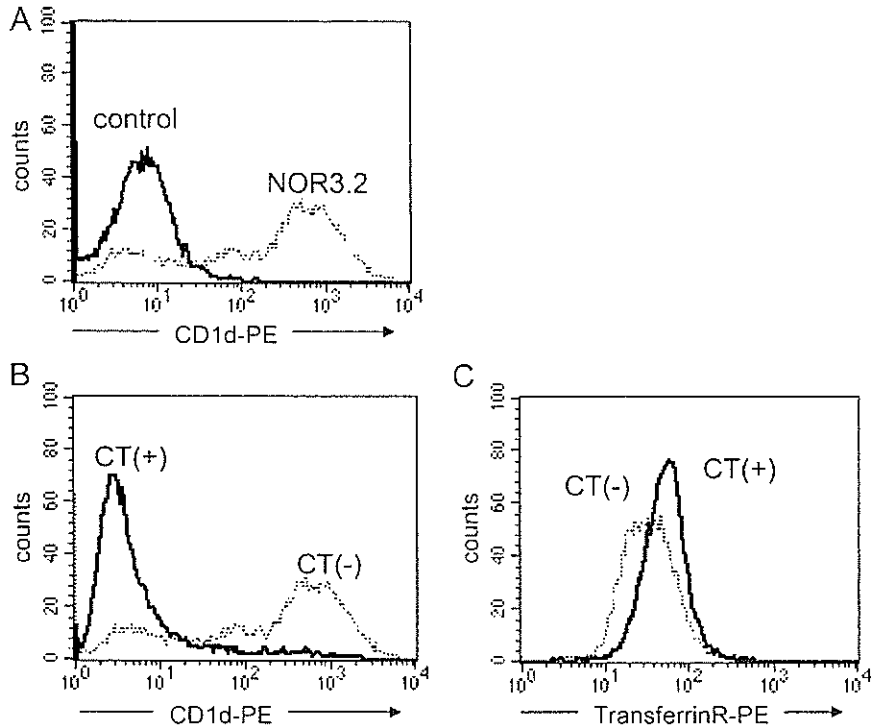

FIGURE 1. ***C. trachomatis* infection down-regulates CD1d surface expression in PURL cells.** *A*, CD1d expression on uninfected PURL cells. Background level staining of the cells with secondary antibody is also shown (*control*). *B*, CD1d expression on PURL cells harvested 24 h post infection with *C. trachomatis* serovar F (*CT(+)*) and uninfected cells (*CT(−)*). The PURL cells were stained with the NOR 3.2 anti-CD1d antibody and a phycoerythrin conjugated goat anti-mouse Ig secondary antibody. *C*, transferrin receptor expression on *C. trachomatis*-infected and uninfected PURL cells. *CT*, *C. trachomatis*.

buffer (11). Protein products were analyzed by Western immunoblotting.

Immunoprecipitation by a His-tagged, Synthetic CD1d Cytoplasmic Tail—Three polypeptides with sequences corresponding to the wild-type CD1d cytoplasmic tail (HHHHHH-RFKRQTSY-QGVL), to a mutated cytoplasmic tail lacking tyrosine and lysine residues (HHHHHH-RFKRQTS*F*QGV*A*), or to a truncated cytoplasmic tail lacking six amino acids (HHHHHH-RFKRQT) (20) were synthesized, His tag conjugated, and purified by high-performance liquid chromatography (New England Peptide, Inc., Gardner, MA). Total cell lysates were incubated with or without the synthesized peptides (0, 20, or 100 μg) in 200 μl of radioimmune precipitation assay buffer for 2 h at 4 °C. Bound proteins were recovered using anti-His tag antibody-conjugated agarose beads (Abcam Inc.), separated by PAGE and immunoblotted with the anti-CPAF c100a mAb.

Fluorescence Deconvolution Microscopy—PURL cells were seeded onto coverslips and infected as above. The ER was visualized using ER tracker Blue-White DPX (Molecular Probes, Eugene, OR) for 30 min at 37 °C. All coverslips were fixed in 4% paraformaldehyde, permeabilized with 0.1% Tween 20, and incubated for 2 h at 37 °C with anti-CD1d 51.1.3 mAb, anti-CD1d NOR3.2 mAb, or anti-CPAF n54b mAb singly, or in combination with anti-chlamydial LPS (clone-3, Accurate, Westbury, NY). Alexa Fluor 568-conjugated anti-mouse IgG1 (51.1.3, NOR3.2, and n54b) or Alexa Fluor 488-conjugated anti-mouse IgG3 (chlamydial LPS) were used as secondary reagents. In some experiments NOR3.2 was directly conjugated with Zenon Alexa Fluor 488 using a mouse IgG1 labeling kit (Molecular Probes) to allow costaining with CPAF. Thereafter, except in ER-Tracker-treated coverslips, cells were counterstained with a 4′,6-diamidino-2-phenylindole (Molecular Probes) nucleic acid stain. Images were obtained with a Leica DMRXA automated upright epifluorescence microscope (Leica Microsystems, Bannockburn, IL); a Sensicam QE charge-coupled device (Cooke Corp., Auburn Hills, MI); and filter sets optimized for Alexa 488 (exciter HQ480/20, dichroic Q495LP, and emitter HQ510/20m), Alexa 568 (exciter 545/30x, dichroic Q570DLP, emitter HQ620/60m), and 4′,6-diamidino-2-phenylindole (exciter 360/40×, dichroic 400DCLP, and emitter GG420LP). Z-axis plane capture, deconvolution, and analysis were performed with Slidebook™ deconvolution software (Intelligent Imaging Innovations, Denver, CO).

RESULTS

To determine how *C. trachomatis* infection affects CD1d expression, flow cytometry was used to analyze its cell-surface expression on PURL epithelial cells, a cell line we immortalized from penile urethra, the most common site of infection in the male. Cells were infected with *C. trachomatis* serovar F in this, and all subsequent experiments, because it is one of the most frequent genital isolates. We observed that CD1d was expressed by the majority of uninfected PURL cells; however, by 24 h post infection, CD1d expression was abrogated in >90% of cells in the *C. trachomatis*-infected cultures (Fig. 1*B*). The loss of CD1d expression was selective, because PURL cells retained, and in fact showed a slight increase in, their expression of transferrin receptor (Fig. 1*C*). PURL cells were then infected with *C. trachomatis* and harvested at various time points (up to 45 h after infection) to biochemically assess the effects of *C. trachomatis* infection on CD1d HC. All isoforms of CD1d HC were recovered using an anti-CD1d mAb (D5) that recognizes the α-region of the CD1d HC regardless of its association with β2m (10, 11). The anti-CD1d D5 mAb precipitated CD1d HC isoforms of ~48 kDa (*open arrowhead*), 45 kDa (*closed arrow*), and 37 kDa (*open arrow*) with distinct patterns depending on infection status and time after *C. trachomatis* infection. (Fig. 2*A*, *panel 1*). In non-infected PURL cells, the 48-kDa CD1d HC predominated, whereas the 45- and 37-kDa forms were present in negligible amounts (*panel 1*, *lane 1*).

CD1d isoforms were altered in the presence of *C. trachomatis* infection in a time-dependent, stepwise fashion (Fig. 2*A*, *panel 1*). The 48-kDa HC was largely converted to a 45-kDa HC

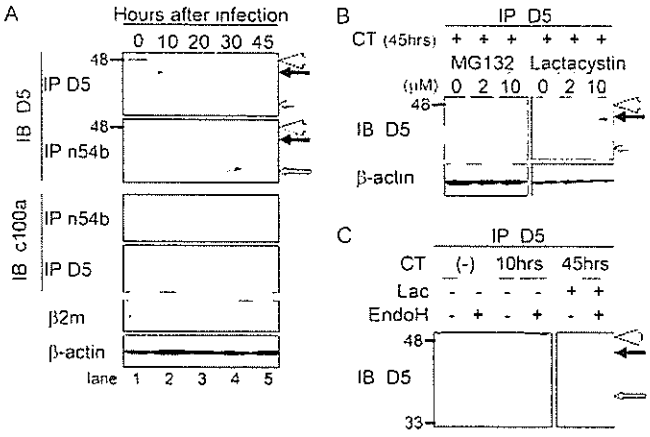

FIGURE 2. **CD1d HC degradation upon *C. trachomatis* infection.** *A*, PURL cells were infected with *C. trachomatis* and harvested at 0, 10, 20, 30, and 45 h p.i. Total cell lysates were subjected to IP using anti-CD1d (*D5*) or anti-CPAF n-fragment (*n54b*) mAbs. Precipitated proteins were separated by PAGE and immunoblotted with anti-CD1d (*D5*) or anti-CPAF c-fragment (*c100a*) mAbs. The mAb pairs (D5–D5, n54b–D5, n54b–c100a, or D5–c100a) when used sequentially for IP and IB, isolated total CD1d HC, CPAF-bound CD1d HC, total CPAF, or CD1d-bound CPAF, respectively. *Open arrowheads*, *closed arrows*, and *open arrows* indicate the 48-, 45-, and 37-kDa HC bands, respectively. Protein levels of β2m and β-actin (loading control) in total cell lysates were detected by Western immunoblotting. *B*, PURL cells were infected as in *A* and exposed to the proteasome inhibitors, MG132 (*left*) or lactacystin (*right*) at the indicated concentrations for 45 h. Total cell lysates were used for IP and IB with the anti-CD1d (D5) mAb as in *A*. *Arrow/arrowheads* indicate HC bands as in *A*. *C*, D5-precipitated proteins from *C. trachomatis*-infected and non-infected lactacystin (*Lac*)-treated cells were treated with endoglycosidase-H (*EndoH*). Endoglycosidase-H-treated and control proteins were used for IP and IB with the anti-CD1d (*D5*) mAb as in *A*. *Arrow/arrowheads* indicate HC bands as in *A*. *CT*, *C. trachomatis*.

form between 10 to 20 h post infection (p.i.), and this was accompanied by a decrease in β2m protein levels (Fig. 2*A*, *panels 1* and *5*). To confirm the glycosylation status of the 45-kDa HC, the isoform was digested by endoglycosidase-H (Fig. 2*C*). The 45-kDa CD1d HC was sensitive to endoglycosidase-H and represents an immature glycosylated CD1d that may include β2m-unassembled HCs.

The amount of detectable, 45-kDa, glycosylated CD1d HC protein decreased by 20 h p.i. By 30 h p.i., it was no longer detectable. In its place, a 37-kDa non-glycosylated CD1d HC form began to accumulate at 20 h p.i. This isoform predominated at 30 h but was nearly undetectable by the end of the infectious cycle.

We hypothesized that the degradation of CD1d HCs in the presence of *C. trachomatis* infection may involve the *C. trachomatis*-specific proteasomal activity, CPAF (6). To address this possibility, we used coimmunoprecipitation (IP) to search for physiologic interactions between CPAF and CD1d HCs (Fig. 2*A*, *panels 2–4*). Using combinations of the anti-CD1d D5 mAb and mAbs against the C-terminal (c100a) or N-terminal (n54b) fragments of CPAF we could demonstrate association between CPAF and CD1d and follow these associations through the infectious cycle. CPAF-bound proteins and CPAF itself were immunoprecipitated with the anti-CPAFn n54b mAb, separated by PAGE, and immunoblotted with anti-CD1d D5 (*panel 2*) or anti-CPAFc c100a (*panel 3*) mAbs. In turn, CD1d-associated proteins were recovered with the anti-CD1d D5 mAb, separated by PAGE and immunoblotted with anti-CPAFc c100a mAb (*panel 4*). Experiments using primary IP with anti-CD1d D5 and anti-CPAFn n54b mAbs demonstrated that CD1d HCs and CPAF interacted with each other physiologically (Fig. 2*A*, *panels 2* and *4*). Furthermore, CPAF preferentially associated with the 45-kDa immature glycosylated CD1d and 37-kDa non-glycosylated CD1d but not the 48-kDa mature glycosylated CD1d HC (Fig. 2*A*, *panel 2*). CPAF binding to CD1d HC was first detected at 20 h p.i. By 30 h p.i., the CPAF-associated immature glycosylated CD1d was undetectable. In parallel, the levels of the CPAF-associated non-glycosylated CD1d increased transiently at 30 h p.i. and decreased to nearly undetectable levels by 45 h p.i. Primary CPAF IPs (*panels 3* and *4*) confirmed the findings of primary CD1d IPs. CPAF was first detected at 10 h p.i., and the levels of total and CD1d-associated CPAF increased by 20 h p.i. and then decreased by 45 h p.i.

To assess the role of proteasomal activity in *C. trachomatis*-associated degradation of CD1d HC, *C. trachomatis*-infected cells were exposed to the cytosolic proteasome inhibitor, MG132 (*left panel*) and to lactacystin (*right panel*) (Fig. 2*B*). Total CD1d HC was detected by IP-IB with the anti-CD1d D5 mAb. In the absence of proteasomal inhibition, CD1d HCs could not be detected at 45 h p.i. In the presence of either MG132 or lactacystin, the 37-kDa non-glycosylated CD1d was detectable, and levels of this HC increased with increasing inhibitor dose. In turn, in the presence of lactacystin, but not MG132, the 45-kDa immature glycosylated CD1d could be detected, and levels of this HC increased with lactacystin dose. The rescued 45-kDa HC form was confirmed to be sensitive to endoglycosidase-H. The immature glycosylated CD1d HC was degraded without deglycosylation (Fig. 2*C*).

As illustrated in *panels 3* and *4* of Fig. 2*A*, CD1d-associated CPAF was no longer detectable by 45 h p.i., despite the continued presence of some CPAF protein. Indeed, CD1d-associated CPAF was rescued by both MG132 and lactacystin, indicating that at least the classic cytosolic proteasome is involved in the degradation of CPAF together with the CD1d HC (Fig. 3*A*).

Fractionation experiments have demonstrated that CPAF is localized to the cytosol and is active in this location (4, 6). However, neither properly assembled nor aberrant forms of CD1d are normally present in the cytosol (11, 12). Still, CD1d and CPAF interact physiologically. We hypothesized that CPAF associates with CD1d HCs via a site on the CD1d cytoplasmic tail. To address this hypothesis, we synthesized three peptides with amino acid sequences corresponding to the 12 amino acids that comprise the entire wild-type CD1d cytoplasmic tail (RFKRQTSYQGVL), to a mutated cytoplasmic tail lacking tyrosine and lysine residues (RFKRQTS*F*QGV*A*), and to a truncated cytoplasmic tail lacking six amino acids (RFKRQT) (20). All peptides were conjugated to a His tag. Total cell lysates from infected and control PURL cells were incubated with the synthetic His-tagged CD1d cytoplasmic tail, and peptide-associated proteins were recovered with an anti-His tag antibody. Western immunoblotting of the precipitated proteins demonstrated that CPAF interacted physically with the CD1d cytoplasmic tail, and these interactions occurred in a dose-dependent manner (Fig. 3*B*). In comparison to the CPAF band precipitated by the wild-type peptide (*wt*), CPAF was barely detectable after precipitation by the point-mutated peptide

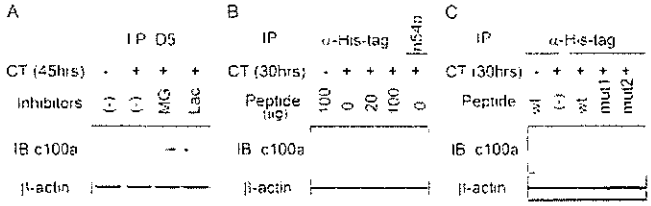

FIGURE 3. **CPAF rescue by proteasome inhibitors and CPAF interaction with CD1d.** *A*, PURL cells were infected as in Fig. 1*A* and exposed to 10 μM MG132, 10 μM lactacystin, or vehicle control for 45 h. CD1d-bound CPAF was immunoprecipitated with the anti-CD1d (D5) antibody. Immunoprecipitants were separated by PAGE and immunoblotted with the anti-CPAFc (c100a) mAb. β-Actin in total cell lysates (loading control) was detected separately using Western immunoblotting. *B*, an His tag-conjugated peptide with amino acid sequence corresponding to the entire cytoplasmic tail of the human CD1d HC was synthesized and purified by high-performance liquid chromatography. Various amounts of peptide (0, 20, or 100 μg per 200 μl of radioimmune precipitation assay buffer) were incubated with total cell lysates from non-infected and *C. trachomatis*-infected cells. Peptide-bound proteins were recovered with an anti-His tag antibody. Immunoprecipitants were separated by PAGE and immunoblotted with the anti-CPAFc c100a mAb. Precipitatants using the anti-CPAFn n54b mAb served as a positive control. *C*, 100 μg of three synthetic peptides (wild-type peptide (*wt*), a point-mutated peptide lacking tyrosine and lysine residues (*mut1*), or a truncated peptide lacking cytoplasmic six amino acids (*mut2*)), were used for peptide precipitations as in Fig. 3*B*. Immunoprecipitants were separated by PAGE and immunoblotted with the anti-CPAFc c100a mAb. *CT*, *C. trachomatis*.

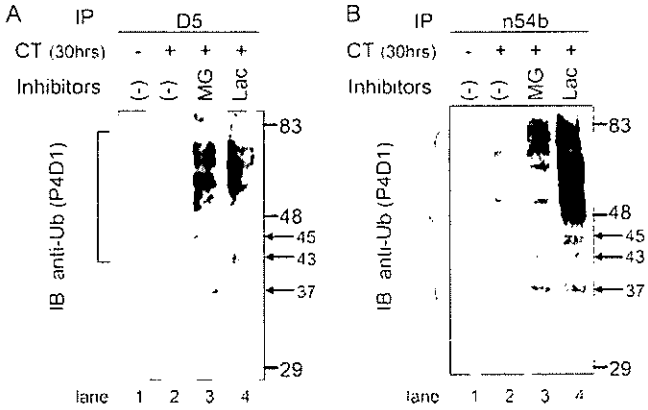

FIGURE 4. **CD1d HC and CPAF are ubiquitinated prior to degradation.** PURL cells were infected with *C. trachomatis* as in Fig. 1 and exposed to 10 μM of MG132 (*MG*), 10 μM lactacystin (*Lac*), or vehicle control for 30 h. Total cell lysates from non-infected and *C. trachomatis*-infected cells were immunoprecipitated with either anti-CD1d (*D5*) (*A*) or anti-CPAFn (*n54b*) mAbs (*B*) as described in Fig. 1*A*. Precipitated proteins were separated by PAGE and immunoblotted with a peroxidase-conjugated mouse anti-ubiquitin antibody (*P4D1*). *Closed arrows* indicate exact molecular weights. Standard molecular size markers are shown. Ubiquitinated CD1d/CD1d-associated proteins or CPAF/CPAF-associated proteins are shown using a *bracket* or *brace*, respectively. *CT*, *C. trachomatis*.

(*mut1*) and undetectable after precipitation with the truncated peptide (*mut2*) (Fig. 3*C*). These data suggest that CPAF interacts directly or indirectly to CD1d HC via sites on the CD1d cytoplasmic tail.

The classic cellular proteasome requires ubiquitination of host *N*-linked glycoproteins prior to their degradation (21). PURL cells were infected with *C. trachomatis* and exposed to proteasome inhibitors. Total cell lysates harvested at 30 h pi were subjected to IP with either anti-CD1d D5 (Fig. 4*A*) or anti-CPAFn n54b (Fig. 4*B*) mAbs. Immunoprecipitants were separated by PAGE and immunoblotted with a peroxidase-conjugated anti-ubiquitin antibody. Ubiquitinated CD1d HCs were not detected in non-infected cells (Fig. 4*A*, *lane 1*) and were

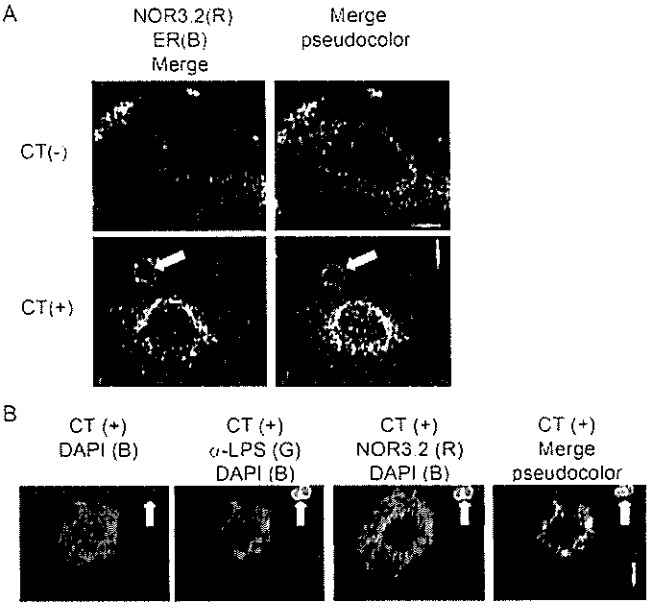

FIGURE 5. **Redistribution of CD1d HC in *C. trachomatis*-infected cells.** PURL cells were infected with *C. trachomatis* as described in Fig. 1*A*. At 24 h post infection. *A*, dual labeling of infected and control cells was performed with an anti-CD1d mAb (NOR3.2, *red*) and ER tracker (*blue*) and visualized by fluorescence deconvolution microscopy (*left panels*). Pseudocolor images represent the intensity of colocalization of the ER with respect to CD1d (*right panels*). The pseudocolor spectrum varies from *blue* (no colocalization) to *red* (full colocalization). *B*, the *C. trachomatis*-infected PURL cells were labeled with 4′,6-diamidino-2-phenylindole (*DAPI*, *blue*), anti-chlamydial LPS (*green*), and NOR3.2 (*red*) (*three left panels*). The pseudocolor image represents the intensity of colocalization of chlamydial LPS with respect to CD1d (*right panel*). *Arrows* indicate chlamydial inclusion. *CT*, *C. trachomatis*.

barely detectable in *C. trachomatis*-infected cells that were not exposed to proteasome inhibitors (Fig. 4*A*, *lane 2*). In contrast, in the presence of proteasome inhibitors, ubiquitinated proteins accumulated in *C. trachomatis*-infected cells. Use of protein size markers and size analysis confirmed that the molecular weights of the ubiquitinated CD1d and CPAF bands were as expected. Ubiquitinated CD1d HCs were observed as a ladder of signals with molecular masses greater than ~45 kDa (Fig. 4*A*, *lanes 3* and *4*). The 37- and 43-kDa bands may represent ubiquitinated proteins coprecipitated with CD1d, possibly including ubiquitinated CPAF N and C terminus fragments (Fig. 4*A*). Ubiquitinated CPAF-associated proteins, including CD1d HCs, were observed as a ladder of signals with molecular masses greater than ~45 kDa (Fig. 4*B*, *lanes 3* and *4*). The amounts of ubiquitinated CPAF or CPAF-associated proteins, including CD1d HCs, were greater after exposure to lactacystin than to MG132 (Fig. 4, *A* and *B*).

To visually document the effect of *C. trachomatis* infection on CD1d intracellular trafficking, immunofluorescence microscopy was first performed with an anti-CD1d mAb (NOR3.2) that reacts with total CD1d HCs and either an ER-specific marker (ER tracker) or an anti-chlamydial LPS mAb (Fig. 5). In non-infected PURL cells, NOR3.2-reactive CD1d was detected throughout the intracellular space, with increased accumulation near the cell surface (Fig. 5*A*, *upper images*). In contrast, the majority of CD1d molecules in *C. trachomatis*-infected PURL cells localized to the perinuclear area near the ER (Fig. 5*A*, *lower images*). In addition, CD1d was present in

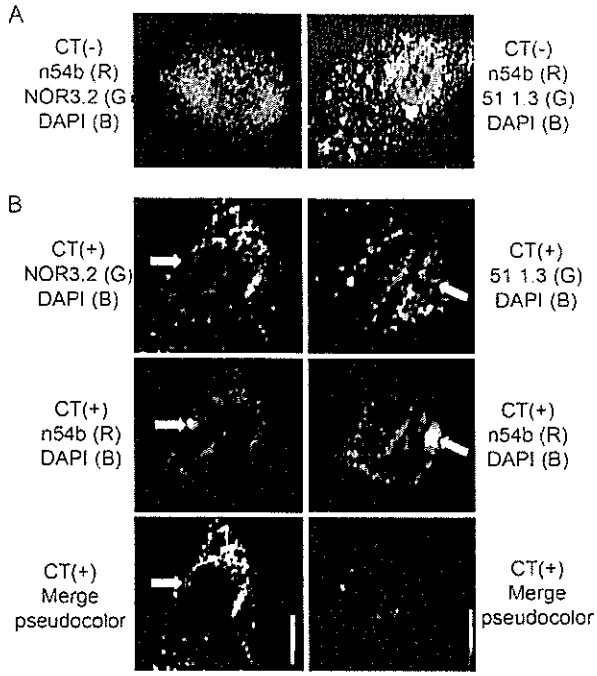

FIGURE 6. **CPAF distribution in *C. trachomatis*-infected cells.** PURL cells were infected with *C. trachomatis* as described in Fig. 1*A*. At 24 h post infection control cells (*A*) and infected cells (*B*) were costained with anti-CD1d (CD1d HC, NOR3.2-reactive (*left panels*) or properly folded mature glycosylated CD1d, 51.1.3-reactive (*right panels*)) mAbs (*green*), anti-CPAF (n54b) mAb (*red*), and 4′,6-diamidino-2-phenylindole (*blue*) and visualized by fluorescence deconvolution microscopy. Pseudocolor images in *B* represent the intensity of colocalization of CPAF with respect to CD1d. The pseudocolor spectrum varies from *blue* (no colocalization) to *red* (full colocalization). *Arrows* indicate chlamydial inclusion. *CT*, *C. trachomatis*.

infected cells in a distinct ring-shaped intracellular distribution that correlates morphologically with the chlamydial inclusion. CD1d and ER signals partially colocalized in the perinuclear area, suggesting that some forms of CD1d are present within the ER, but the majority of CD1d localized to the cytosol surrounding the ER (Fig. 5*A*, *right images*). Dual labeling for CD1d and chlamydial LPS verified the colocalization of CD1d and chlamydial elements within the chlamydial inclusion (Fig. 5*B*, *green* to *red pseudocolor*). These immunofluorescence microscopy studies thus support our flow cytometry and biochemical data that CD1d HC in *C. trachomatis*-infected cells fails to traffic efficiently to the cell surface. Rather, by 24 h p.i., the majority of CD1d HCs can be found in the cytosol near the ER, although some HCs localize within the ER and around chlamydial inclusion. CD1d HC appears to be targeted toward two degradation pathways: one ER-associated and one *Chlamydia*-mediated.

The anti-CD1d 51.1.3 mAb preferentially recognizes a conformational epitope associated with CD1d maturity (10, 11). This allowed us to discriminate the effects of *C. trachomatis* infection on properly folded mature glycosylated CD1d (51.1.3-reactive) from the effects on total CD1d HCs (NOR3.2-reactive) (Fig. 6). A pseudocolor rendering demonstrated moderate colocalization of CPAF and NOR3.2-reactive CD1d HC (Fig. 6*B*, *bottom left panel*) and confirmed our biochemical data showing the physiologic interaction of cytosolic CPAF with the CD1d HC. The distribution of the CPAF-CD1d complex was similar to that of total CD1d HC shown in Fig. 5. In the *right panel* of Fig. 6*A*, 51.1.3-reactive mature glycosylated CD1d is again noted throughout the intracellular space and on the cell surface in uninfected cells. By 24 h p.i., mature glycosylated CD1d localized almost exclusively to the perinuclear area (Fig. 6*B*, *right panels*). Signals for CPAF also localize to the perinuclear area and in the area of the chlamydial inclusion. Pseudocolor rendering (*bottom right panel*) indicated that there is no colocalization of CPAF with 51.1.3-reactive mature glycosylated CD1d. These patterns differed significantly from those for NOR3.2-reactive CD1d HC (*left panels*) and demonstrate that mature glycosylated CD1d is neither bound to CPAF nor associated with the chlamydial inclusion.

DISCUSSION

This study demonstrates that CD1d molecules are decreased on the surface of *C. trachomatis*-infected cells, although CD1d mRNA levels were not altered when compared with those in non-infected cells (data not shown). The three described isoforms of CD1d HC protein were here observed in distinctive patterns that depended upon the infection status and the time after *C. trachomatis* infection. The 45-kDa glycosylated CD1d HC, rather than the 48-kDa mature glycosylated CD1d HC, is the predominant isoform present between 10 and 20 h p.i. This was accompanied by a decrease in β2m protein levels. The reduction in recoverable β2m in *C. trachomatis*-infected cells has been reported to result from degradation of the transcription factor, RFX5, by CPAF (4). Zhong G *et al.* reports that CPAF is secreted into cytosol after 24 h of infection in HeLa cell (4, 6). The exact timing of the secretion of CPAF in our experiments may be characteristic of our infected cell type and the infecting *C. trachomatis* serovar and may therefore differ from the timing seen in similar experiments performed by others. Here, CPAF secretion started at 10 h p.i. and accumulated in the cytosol by 24 h p.i. as demonstrated visually in Fig. 6. Because the effect of CPAF on β2m through RFX5 is very rapid (within 30 min) (4), the appearance of CPAF at 10 h p.i. could result in our observed decrease in β2m between 10 to 20 h p.i. In β2m-deficient cells, surface-expressed CD1d HCs are glycosylated, but their carbohydrate side chains are incompletely modified. These CD1d HCs migrate at ~45 kDa (11), as do the β2m-unassembled immature glycosylated CD1d shown in our experiments. Notably, CD1d HC carbohydrate modification and trafficking to the cell surface is delayed in β2m-deficient cells (11). This effect is consistent with our immunohistochemical data. The delayed exit of immature glycosylated CD1d from the ER should facilitate CPAF-associated direction of CD1d to degradation. Finally cell-surface CD1d was clearly down-regulated in *C. trachomatis*-infected cells analyzed by flow cytometry.

The classic cellular proteasome requires removal of *N*-linked glycans from aberrant cytosolic glycoprotein targets prior to their degradation (13). However, in our experiments, lactacystin rescued a 45-kDa CD1d HC that remained sensitive to endoglycosidase-H. This immature glycosylated CD1d HC appears to be degraded without deglycosylation. Because MG132 was not able to rescue this immature glycosylated CD1d isoform, we propose that it is degraded by CPAF rather than by the classic cellular proteasome.

In contrast, the 37-kDa non-glycosylated isoform of CD1d was rescued by both proteasome inhibitors. Because the CPAF-mediated proteolytic pathway can't be inhibited by MG132 (4), the non-glycosylated 37-kDa CD1d HC must be degraded at least partially by the classic cytosolic proteasome. The degradation process for this isoform, including ubiquitination and deglycosylation, suggest it represents an intermediate in the classic proteolytic pathway for degrading aberrant *N*-linked glycoproteins (13, 21). The *C. trachomatis*-infected epithelial cells shown here represent the first model system to allow detection of all three isoforms of the CD1d HC. The experimental system suggests that all isoforms may be pathophysiologically relevant.

Immunostaining data support a model in which CPAF binds to immature glycosylated CD1d and non-glycosylated CD1d and dislocates them into the cytosol surrounding the ER and the chlamydial inclusion. Here, it is degraded in a CPAF-dependent manner that can be distinguished from pathways for classic cytosolic proteasomal degradation.

Interestingly, our ubiquitination experiments demonstrated that the amounts of ubiquitinated CPAF-associated proteins were greater after exposure to lactacystin than after exposure to MG132. However, there was no difference in the amount of rescued CPAF between exposure to MG132 and lactacystin (Fig. 3*A*). These data suggest that CPAF target proteins could be ubiquitinated prior to degradation by a CPAF-associated proteolytic pathway. Ubiquitinated CD1d HC could be degraded by both classic and CPAF-associated pathways, because those were rescued equally by MG132 and lactacystin. In initial descriptions of chlamydial proteasome-like activity, the authors noted the possibility that *C. trachomatis* could also co-opt cellular cytosolic proteolytic pathways to degrade host transcription factors (4, 6). Our data clearly demonstrate that *C. trachomatis* not only provides its own mechanism for CD1d degradation but also uses the classic proteolytic pathway for degrading aberrant *N*-linked glycoproteins to inhibit CD1d trafficking to the cell surface. CPAF is involved in both pathways.

We propose the following model for CD1d proteolysis in *C. trachomatis*-infected cells (Fig. 7). Cytosolic CPAF interacts with CD1d via cytoplasmic tail of the CD1d HC. This triggers dislocation of the CD1d HC into the cytosol where it is further processed along two distinct pathways. In one, glycosylated HC in the cytosol is ubiquitinated and deglycosylated. Ubiquitinated, deglycosylated CD1d and CPAF are directed toward degradation by the classic cytosolic proteasome. Immature glycosylated CD1d HC is degraded by CPAF-associated mechanisms that are distinct from those of the cytosolic proteasome.

Does *C. trachomatis* target CD1d HC for degradation as a means to evade immune recognition? In responses to some microbes, the rapid effects of CD1d-restricted NKT cells do not require recognition of microbial specific antigens (16–18). Instead, NKT cells can be activated in response to self-antigen presented by CD1d, and these actions are amplified by interleukin-12 derived from dendritic cells (16). Certainly, a reduced expression of CD1d at the cell surface could prevent *C. trachomatis*-infected cells from such an attack. It was recently demonstrated that Kaposi sarcoma-associated herpesvirus reduces

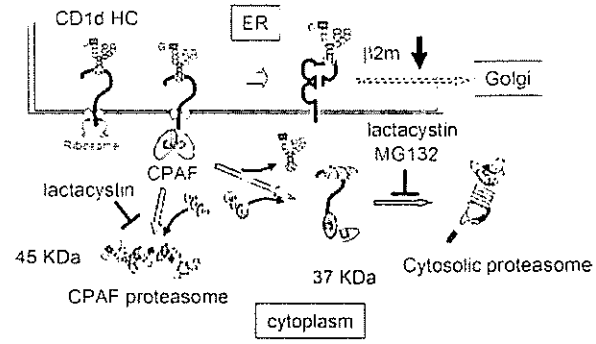

FIGURE 7. **Putative proteolytic degradation pathways for CD1d HCs upon *C. trachomatis* infection.** In *C. trachomatis*-infected cells, β2m-unassembled CD1d HC forms accumulate in the ER due to degradation of RFX5 by CPAF. CPAF secreted from the chlamydial inclusion into the cytosol interacts with the CD1d HC via cytoplasmic tail of the CD1d and CPAF is ubiquitinated. The binding of CPAF triggers dislocation of the 45-kDa immature glycosylated form of CD1d into the cytosol. One proteolytic pathway involves the conventional cellular proteasome. Glycosylated CD1d HC is ubiquitinated in the cytosol (ubiquitin ligase), and deglycosylated (peptide *N*-glycosidase) to create the 37-kDa non-glycosylated CD1d molecule. CPAF and the ubiquitinated, deglycosylated CD1d HC are degraded by the cytosolic proteasome. The alternative proteolytic pathway involves CPAF-mediated degradation. The 45-kDa immature glycosylated CD1d HC interacts with CPAF. CPAF targets the CD1d HC for degradation by a proteolytic activity distinct from that of the cytosolic proteasome. *Green symbols* indicated multiubiquitins.

cell-surface expression of CD1d via ubiquitination of the CD1d HC on its cytoplasmic tail (15). This, in turn, impairs CD1d-restricted T cell activation toward virally infected cells (15). Herpes simplex virus-1 down-regulates cell-surface CD1d expression by inhibition of CD1d recycling (22). Human immunodeficiency virus-1 Nef protein reduces cell-surface CD1d expression by binding to the cytoplasmic tail of CD1d HC, and this accompanies a decreased NKT cell activation (20). In *C. trachomatis*-infected PURL cells, CD1d degradation is accompanied by a suppression of CD1d-mediated cytokine secretion, including the production of interleukin-12.[3] Regardless of whether chlamydial antigens are presented by CD1d, the disruption of CD1d expression in *C. trachomatis*-infected cells may interfere with rapid and essential innate immune responses.

Acknowledgments—We are grateful to Dr. G. Zhong for his kind gifts of anti-CPAF antibodies and purified CPAF c-fragment proteins, the Morphology and Imaging Core of the Louisiana State University Health Sciences Center Gene Therapy Program for facilitation of the fluorescent deconvolution microscopy, Dr. J. Nichols and J. Niles at University of Texas Medical Branch for facilitation of the flow cytometry studies, to C. D. McGahan and Dr. L. S. Graziadei for editorial assistance, and to Dr. Priscilla Wyrick for critical reading of the manuscript.

REFERENCES

1. Cates, W Jr. and Wasserheit, J. N. (1991) *Am. J. Obstet Gynecol.* 164, 1771–1781
2. Hogan, R. J., Mathews, S. A. Mukhopadhyay, S., Summersgill, J. T and Timms, P. (2004) *Infect. Immun.* 72, 1843–1855
3. Beatty, W L., Morrison, R. P., and Byrne, G. I. (1994) *Microbiol. Rev.* 58, 686–699

[3] K. Kawana and D. J. Schust, unpublished observation.

4. Zhong, G., Liu, L., Fan, T., Fan, P., and Ji, H. (2000) *J. Exp. Med.* 191, 1525–1534
5. Zhong, G., Fan, T., and Liu, L. (1999) *J. Exp. Med.* 189, 1931–1938
6. Zhong, G., Fan, P., Ji, H., Dong, F., and Huang, F. (2001) *J. Exp. Med.* 193, 935–942
7. Dong, F., Pirbhai, M., Zhong, Y., and Zhong, G. (2004) *Mol. Microbiol.* 52, 1487–1494
8. Bendelac, A., Lantz, O., Quimby, M. E., Yewdell, J. W., Bennink, J. R., and Brutkiewicz, R. R. (1995) *Science.* 268, 863–865
9. Taniguchi, M., and Nakayama, T. (2000) *Semin. Immunol.* 12, 543–550
10. Balk, S. P., Burke, S., Polischuk, J. E., Frantz, M. E., Yang, L., Porcelli, S., Colgan, S. P., and Blumberg, R. S. (1994) *Science* 265, 259–262
11. Kim, H. S., Garcia, J., Exley, M., Johnson, K. W., Balk, S. P., and Blumberg, R. S. (1999) *J. Biol. Chem.* 274, 9289–9295
12. Kang, S. J., and Cresswell, P. (2002) *J. Biol. Chem.* 277, 44838–44844
13. Hirsch, C., Blom, D., and Ploegh, H. L. (2003) *EMBO J.* 22, 1036–1046
14. Skold, M., and Behar, S. M. (2003) *Infect. Immun.* 71, 5447–5455
15. Sanchez, D. J., Gumperz, J. E., and Ganem, D. (2005) *J. Clin. Invest.* 115, 1369–1378
16. Brigl, M., Bry, L., Kent, S. C., Gumperz, J. E., and Brenner, M. B. (2003) *Nat. Immunol.* 4, 1230–1237
17. Mattner, J., Debord, K. L., Ismail, N., Goff, R. D., Cantu, C., 3rd, Zhou, D., Saint-Mezard, P., Wang, V., Gao, Y., Yin, N., Hoebe, K., Schneewind, O., Walker, D., Beutler, B., Teyton, L., Savage, P. B., and Bendelac, A. (2005) *Nature* 434, 525–529
18. Gumperz, J. E., Roy, C., Makowska, A., Lum, D., Sugita, M., Podrebarac, T., Koezuka, Y., Porcelli, S. A., Cardell, S., Brenner, M. B., and Behar, S. M. (2000) *Immunity* 12, 211–221
19. Fichorova, R. N., Rheinwald, J. G., and Anderson, D. J. (1997) *Biol. Reprod.* 57, 847–855
20. Cho, S., Knox, K. S., Kohli, L. M., He, J. J., Exley, M. A., Wilson, S. B., and Brutkiewicz, R. R. (2005) *Virology* 337, 242–252
21. Yoshida, Y., Chiba, T., Tokunaga, F., Kawasaki, H., Iwai, K., Suzuki, T., Ito, Y., Matsuoka, K., Yoshida, M., Tanaka, K., and Tai, T (2002) *Nature* 418, 438–442
22. Yuan, W., Dasgupta, A., and Cresswell, P. (2006) *Nat. Immunol.* 7, 835–842

ELSEVIER

Journal of Hepatology 46 (2007) 26–36

Journal of Hepatology

www.elsevier.com/locate/jhep

Serum-derived hepatitis C virus infectivity in interferon regulatory factor-7-suppressed human primary hepatocytes

Hussein H. Aly[1,2,3], Koichi Watashi[2], Makoto Hijikata[2], Hiroyasu Kaneko[2], Yasutugu Takada[1], Hiroto Egawa[1], Shinji Uemoto[1], Kunitada Shimotohno[2,*]

[1] *Graduate School of Medicine, Department of Transplant Surgery, Kyoto University Hospital, Kyoto, Japan*
[2] *Laboratory of Human Tumor Viruses, Institute of Virus Research, Kyoto University, Japan*
[3] *Hepatology Department, National Hepatology and Tropical Medicine Research Institute, Cairo, Egypt*

See Editorial, pages 1–5

***Background/Aims*:** The development of an efficient in vitro infection system for HCV is important in order to develop new anti-HCV strategy. Only Huh7 hepatocyte cell lines were shown to be infected with JFH-1 fulminant HCV-2a strain and its chimeras. Here we aimed to establish a primary hepatocyte cell line that could be infected by HCV particles from patients' sera.

***Methods*:** We transduced primary human hepatocytes with human telomerase reverse transcriptase together with human papilloma virus 18/E6E7 (HPV18/E6E7) genes or simian virus large T gene (SV40 T) to immortalize cells. We also established the HPV18/E6E7-immortalized hepatocytes in which interferon regulatory factor-7 was inactivated. Finally we analyzed HCV infectivity in these cells.

***Results*:** Even after prolonged culture HPV18/E6E7-immortalized hepatocytes exhibited hepatocyte functions and marker expression and were more prone to HCV infection than SV40 T-immortalized hepatocytes. The susceptibility of HPV18/E6E7-immortalized hepatocytes to HCV infection was further improved, in particular, by impairing signaling through interferon regulatory factor-7.

***Conclusions*:** HPV18/E6E7-immortalized hepatocytes are useful for the analysis of HCV infection, anti-HCV innate immune response, and screening of antiviral agents with a variety of HCV strains.

Keywords: Immortalization; Primary hepatocytes; HCV infection; IRF-7; IRF-3; HPV18/E6E7; Innate immune response

1. Introduction

Infection with Hepatitis C virus (HCV) is a serious problem worldwide since 3% of the world's population is chronically infected [1]. Chronic HCV may lead to liver cirrhosis and hepatocellular carcinoma. Current standard therapy utilizes the combination of pegylated interferon-α and ribavirin, which results in a sustained response in only 30–60% of patients [2–5]. Many patients, however, do not qualify for or tolerate standard therapy [6]. Thus, it is important to develop an efficient in vitro infection system for HCV to facilitate the discovery of new anti-HCV strategies. Only Huh7 cell line is permissive for replication, infection and release of the fulminant hepatitis-derived HCV-2a (JFH-1) *strain* and its chimeric derivatives [7–9]. No other hepatocyte cell lines are able to support HCV replication efficiently.

Received 5 June 2006; received in revised form 24 July 2006; accepted 1 August 2006; available online 30 October 2006
* Corresponding author. Tel.: +81 75 751 4000; fax: +81 75 751 3998.
E-mail address: kshimoto@virus.kyoto-u.ac.jp (K. Shimotohno).

0168-8278/$32.00
doi:10.1016/j.jhep.2006.08.018

Normal human hepatocytes are the ideal system in which to study HCV infectivity. When cultured in vitro, however, they proliferate poorly and divide only a few times [10]. Continuous proliferation could be achieved however by introducing oncogenes, such as Simian virus large tumor antigen (SV40 T) [11]. This often resulted in tumor development [12] together with numerical (aneuploidy) and structural (aberrations) chromosome abnormalities [13]. The human papilloma virus E6E7 genes (HPV/E6E7) immortalized multiple cell types that were phenotypically and functionally similar to the parental cells [14–20]. As yet, no human hepatocytes have been immortalized with HPV18/E6E7.

We established a human primary non-neoplastic hepatocyte cell line transduced with the HPV18/E6E7 that retained primary hepatocyte characteristics even after prolonged culture, and were more prone to HCV infection than those cells immortalized with SV40 T antigen. We further improved the susceptibility of HPV18/E6E7-immortalized hepatocytes to HCV infectivity by impairing interferon regulatory factor-7 (IRF-7) expression. These cells are useful to assay infectivity of HCV strains other than JFH-1, HCV replication, innate immune system engagement of HCV, and screening of anti-HCV agents. This infection system using non-neoplastic cells also suggested that IRF-7 plays an important role in eliminating HCV infection.

2. Materials and methods

2.1. Cell cultures

We obtained the approval of the Ethical Committee of Kyoto University for the use of human hepatocytes and sera obtained from HCV-positive patients. Informed consent was obtained from both the hepatocyte donor and HCV-positive patients. Primary hepatocytes (P.H.) were cultured as described [21]. HeLa, 293, Huh-7.5, and PH5CH8 cells were cultured as previously described [22]. For three-dimensional (3D) cultures, Mebiol Gel (Mebiol Inc.) was prepared according to the manufacturer's instructions.

2.2. Plasmids construction

The SV40 T, hTERT and HPV/E6E7 fragments from pAct-SVT, PCX4neo/hTERT, and pLXSN-E6E7 plasmids were inserted into pCSII-EF-RFA plasmid creating the pCSII-EF-SVT, pCSII-EF-hTERT, and pCSII-EF-E6E7 plasmids, respectively. The full-length IRF-3 and IRF-7 genes were cloned by RT-PCR using total RNA isolated from 293 cells as a template and were inserted into pcDNA3 vector. Dominant-negative forms of IRF-3 (DNIRF-3) and IRF-7 (DNIRF-7) were constructed by PCR amplification of the coding region for amino acid residues 108–427 of IRF-3 and 237-514 of IRF-7, respectively. The amplified IRF-3 fragment was cloned into pcDNA3 in frame with a FLAG epitope tag generating pcFLAG-DNIRF-3. The amplified IRF-7 fragment was cloned into pLXSH in frame with HA epitope tag generating pLXSH-HA-DNIRF-7. The pIFNβ promoter-luc and pIFNα promoter-luc plasmids were gifts from Dr. Taniguchi of the Tokyo University. The psiRNA-hIRF-3 and psiRNA-hIRF-7 plasmids were purchased from Invivogen (USA).

2.3. Immunoblot analysis

Immunoblot analysis was performed as described previously [22]. We used anti-SV40 T (Santa Cruz), anti-HPV18/E7 (Santa Cruz), anti-tubulin (Sigma), anti-FLAG (Sigma), and anti-HA (Sigma) antibodies.

2.4. Transfection, small interfering RNA silencing and luciferase assays

Transfection of plasmid DNA was performed using Effectene transfection reagent (Qiagen) as recommended by the manufacturer. The pLXSH-HA-DNIRF-7 plasmid was transfected into the HuS-E/2 clone; transfectants were selected in 100 μg/ml hygromycin B (Gibco). The psiRNA-hIRF-3 and psiRNA-hIRF-7 plasmids were separately transfected into HuS-E/2 cells followed by Zeocin (250 μg/ml) selection. After two weeks of continuous selection, cells were infected with HCV. Luciferase assays were conducted as previously described [22]. The results are presented as relative light units (RLU) normalized to the total content of protein in the cell lysates.

2.5. Reverse transcriptase polymerase chain reaction (RT-PCR) and real-time RT-PCR

Using 250 ng of total RNA as a template, we performed RT-PCR with a one-step RNA PCR kit (Takara) according to the manufacturer's instructions. The primer sets and reaction conditions used are detailed in Table 1. To measure HCV-RNA titers by real-time RT-PCR, we collected RNA from infected wells. Five hundred nanograms of total cellular RNA was analyzed for the quantity of HCV-RNA as previously described [23].

2.6. HCV infection experiment

HCV infection experiment from serum was done as mentioned before [22]. HCV-infected-serums were titrated and 1×10^5 HCV-RNA copies/ml were used for each infection experiment. Concentrated culture medium for HCV/JFH1-producing cells was prepared as previously described [7]. HCV titer in the concentrated medium was measured, adjusted and added to the cells as mentioned above.

2.7. Blocking of HCV infectivity by anti-CD81

Inhibition of HCV infectivity was performed by blocking CD81 as previously described [7].

3. Results

3.1. Establishment of immortalized primary human hepatocytes

Primary hepatocytes were isolated from liver tissue obtained from a 9-year-old male patient with Primary Hyperoxaluria who had undergone liver transplantation. Hepatocytes were left unmanipulated or transduced with CSII-EF-hTERT alone or in combination with CSII-EF-SVT or CSII-EF-E6E7 to enhance the efficiency of immortalization. After six weeks only cells transduced by the combination of hTERT and either LT or HPV18/E6E7 continued to proliferate. Initially appearing colonies with a growth advantage were picked up and expanded. SV40 T-immortalized cell clones were named HuS-T cells and given numbers from 1 to 7,

Table 1
Primer sequences and RT-PCR parameters

Genes	Primer sequence 5′–3′	PCR parameters[a]
HGF	F: AGGAGCCAGCCTGAATGATGA R: CCCTCTGATGTCCCAAGATTAGC	95, 56, 72 1 min, 45 s, 1 min
TGFα	F: ATGGTCCCCTCGGCTGGA R: GGCCTGCTTCTTCTGGCTGGCA	95, 59, 72 45 s, 30 s, 1 min
TGFβ1	F: GCCCTGGACACCAACTATTGCT R: AGGCTCCAAATGTAGGGGCAGG	95, 58, 72 45 s, 30 s, 1 min
TGFβ2	F: GATTTCCATCTACAAGACCACGAGGGACTTGC R: CAGCATCAGTTACATCGAAGGAGAGCCATTCG	95, 58, 72 45 s, 30 s, 1 min
HGFR	F: TGGTCCTTGGCGTCGTCCTC R: CTCATCATCAGCGTTATCTTC	95, 54, 72 30 s, 45 s, 1 min
EGFR	F: CTACCACCACTCTTTGAACTGGACCAAGG R: TCTATGCTCTCACCCCGTTCCAAGTATCG	95, 58, 72 45 s, 30 s, 1 min
TGFβ1R	F: CGTGCTGACATCTATGCAAT R: AGCTGCTCCATTGGCATAC	95 s, 54, 72 30 s, 45 s, 1 min
TGFβ2R	F: TGCACATCGTCCTGTGGAC R: GTCTCAAACTGCTCTGAAGTGTTC	95, 58, 72 45 s, 30 s, 1 min
FGFR	F: ATGTGGAGCTGGAAGTGCCTC R: GGTGTTATCTGTTTCTTTCTCC	95, 54, 72 30 s, 45 s, 1 min
IGF-1R	F: ACCCGGAGTACTTCAGCGCT R: CACAGAAGCTTCGTTGAGAA	95, 54, 72 30 s, 45 s, 1 min
HNF1α	F: GTGTCTACAACTGGTTTGCC R: TGTAGACACTGTCACTAAGG	95, 52, 72 45 s, 30 s, 1 min
HNF1β	F: GAAACAATGAGATCACTTCCTCC R: CTTTGTGCAATTGCCATGACTCC	95, 52, 72 1 m, 45 s, 1 min
HNF3β	F: CACCCTACGCCTTAACCAC R: GGTAGTAGGAGGTATCTGCGG	95, 56, 72 1 m, 45 s, 1 min
HNF4	F: CTGCTCGGAGCCACAAAGAGATCCATG R: ATCATCTGCCACGTGATGCTCTGCA	95, 58, 72 45 s, 30 s, 1 min
Albumin	F: AGTTTGCAGAAGTTTCCAAGTTAGTG R: AGGTCCGCCCTGTCATCAG	95, 55, 72 45 s, 30 s, 1 min
Apolipoprotein-a	F:AGGCTCGGCATTTCTGGCAG R: TATCCCAGAACTCCTGGGTC	95, 55, 72 45 s, 30 s, 1 min
HTF	F: TCGCTACAGCCTTTGCAATG R: TTGAGGGTACGGAGGAGTTCC	95, 55, 72 45 s, 30 s, 1 min
E-cadherin	F: TCCATTTCTTGGTCTACGCC R: TTTGTCCTACCGACTTCCAC	95, 55, 72 45 s, 30 s, 1 min
CYP 1B1	F: CACCAAGGCTGAGACAGTGA R: GCCAGGTAAACTCCAAGCAC	94, 57, 72 30 s, 30 s, 1 min
CYP 2C9	F: GGACAGAGACGACAAGCACA R: TGGTGGGGAGAAGGTCAAT	94, 57, 72 30 s, 30 s, 1 min
CYP 2B	F: GGCACACAGCCAAGTTTACA R: CCAGCAAAGAAGAGCGAGAG	94, 57, 72 30 s, 30 s, 1 min
CYP 3A4	F: TGTGCCTGAGAACACCAGAG R: GCAGAGGAGCCAAATCTACC	94, 57, 72 30 s, 30 s, 1 min
CYP 2E1	F: CCGCAAGCATTTTGACTACA R: GCTCCTTCACCCTTTCAGAC	94, 57, 72 30 s, 30 s, 1 min
CYP 1A1	F: AGGCTTTTACATCCCCAAGG R: GCAATGGTCTCACCGATACA	94, 57, 72 30 s, 30 s, 1 min
GAPDH	F: CCATGGAGAAGGCTGGGG R: CAAAGTTGTCATGGATGACC	95, 8, 72 45 s, 30 s, 1 min

Table 1 (*continued*)

Genes	Primer sequence 5′–3′	PCR parameters[a]
CD81	F: CTCAACTGTTGTGGCTCCAAC R: CCAATGAGGTACAGCTTCCC	95, 55, 72 45 s, 30 s, 1 min
TLR3	F: GATCTGTCTCATAATGGCTTG R: GACAGATTCCGAATGCTTGTG	95, 55, 72 45 s, 30 s, 1 min
TLR7	F: CCAGACATCTCCCCAGCGTC R: GGCAAAACAGTAGGGACGGC	95, 55, 72 45 s, 30 s, 1 min
TLR8	F: CTGTGAGTTATGCGCCGAAG R: CGGGATTTCCGTTCTGGTGC	95, 55, 72 45 s, 30 s, 1 min
Myd88	F: GGTCTCCTCCACATCCTCCC R: CCAGCTTGGTAAGCAGCTCG	95, 55, 72 45 s, 30 s, 1 min
IRF3	F: GAACCCCAAAGCCACGGATC R: CCTCCCGGGAACATATGCAC	95, 55, 72 45 s, 30 s, 1 min
IRF7	F: GTGCTGTTCGGAGAGTGGCTC R: CAGCCCAGGCCTTGAAGATG	95, 55, 72 45 s, 30 s, 1 min

CYP, cytochrome P450; EGFR, epidermal growth factor receptor; F, forward primer; FGFR, fibroblast growth factor receptor; GAPDH, glyceraldehyde phosphate dehydrogenase; HGF, hepatocyte growth factor; HGFR, hepatocyte growth factor receptor; HNF, hepatocyte nuclear factor; HTF, human transferrin; IGF-1R, insulin-like growth factor-type I receptor; IRF, interferon regulatory factor; R, reverse primer; TGF, transforming growth factor; TGFR, transforming growth factor receptor; TLR, toll like receptor.

[a] Temperatures are tabulated in the first lane in degrees celsius and the corresponding times in the second lane. Performing one-step RT-PCR, reverse transcription was carried out at 42 °C for 20 min with a pre-PCR denaturation at 95 °C for 10 min.

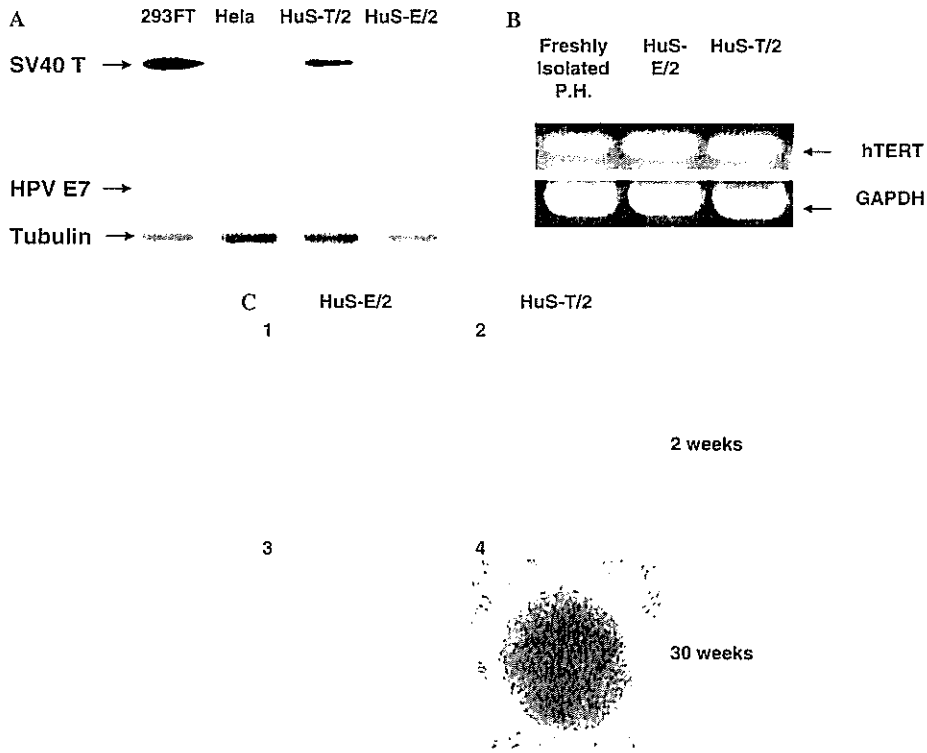

Fig. 1. (A) Immunoblot detection of SV40 T and HPV E7 expression in HuS-T/2 and HuS-E/2 cells, respectively. 293-FT and HeLa cells were used as positive controls for SV40 T and HPV E7 expression, respectively. The specific bands representing the targets are indicated. Detection of tubulin expression in all cells served as an internal control. (B) Human Telomerase Reverse Transcriptase (hTERT) expression was examined by RT-PCR in freshly isolated hepatocytes and the HuS-E/2 and HuS-T/2 cell lines. GAPDH expression was used as an internal control. The hTERT-specific bands are shown. (C) Morphological characteristics of HuS-E/2 and HuS-T/2 cells after two (panels 1 and 2) and 30 (panels 3 and 4) weeks in culture. [This figure appears in colour on the web.]

while the HPV18/E6E7-immortalized clones were named HuS-E cells and given numbers from 1 to 4. Expression of SV40 T and HPV E7 proteins was detected in the appropriate cells by immunoblot analysis (Fig. 1A). In both immortalized cell lines, expression of hTERT-mRNA was enhanced in comparison to non-transduced, freshly isolated hepatocytes as determined by RT-PCR (Fig. 1B). HuS-E cells were larger in size and exhibited slower growth than HuS-T cells (Fig. 1C).

3.2. Characterization of HuS-E and HuS-T immortalized hepatocytes

The HuS-E/2 and HuS-T/2 clones demonstrated the highest expression of hepatocyte-specific markers and transcription factors by RT-PCR (data not shown); these cells were used as representative for each group in this study. To address if HuS-E/2 and HuS-T/2 maintained similar characteristics as primary hepatocytes, they were both cultured continuously for 30 weeks and the expression profiles of a variety of growth factors (Fig. 2A), growth factor receptors (Fig. 2B), hepatocyte-specific nuclear factors (Fig. 2C), albumin, apolipoprotein-A1, transferrin (Fig. 2D), cytochrome p450 (CYP) genes (Fig. 2E), and GAPDH were compared with freshly isolated primary hepatocytes after isolation or two weeks of culture, Huh-7.5 cells, and 293 cells. After two weeks in culture, the expression of nearly all examined genes was similar between freshly isolated hepatocytes and the HuS-E/2 cell line. HuS-E/2 cells, however, exhibited higher expression of TGFβ2 (Fig. 2A), TGFβ2R, and HGFR (Fig. 2B) and lower expression of CYP 3A4 and 2C9 (Fig. 2E) in comparison to freshly isolated hepatocytes. Primary hepatocytes displayed reduced expression of TGFβ1 and TGFβ2 (Fig. 2A) and a loss of CYP1A1 expression (Fig. 2E) after two weeks of culture. HuS-E/2 cells exhibited higher expression of HGF (Fig. 2A), HGF receptor (Fig. 2B), HNF-4, (Fig. 2C), albumin, apolipoprotein-A1, HTF, and E-cadherin (Fig. 2D) in comparison to HuS-T/2 cells. Expression of CYP 3A4 (Fig. 2E) was lost from both HuS-T/2 and HuS-E/2 cells, while HuS-T/2 cells also lost the expression of HNF-1α (Fig. 2D), and CYPs 2B, 2E1 (Fig. 2E).

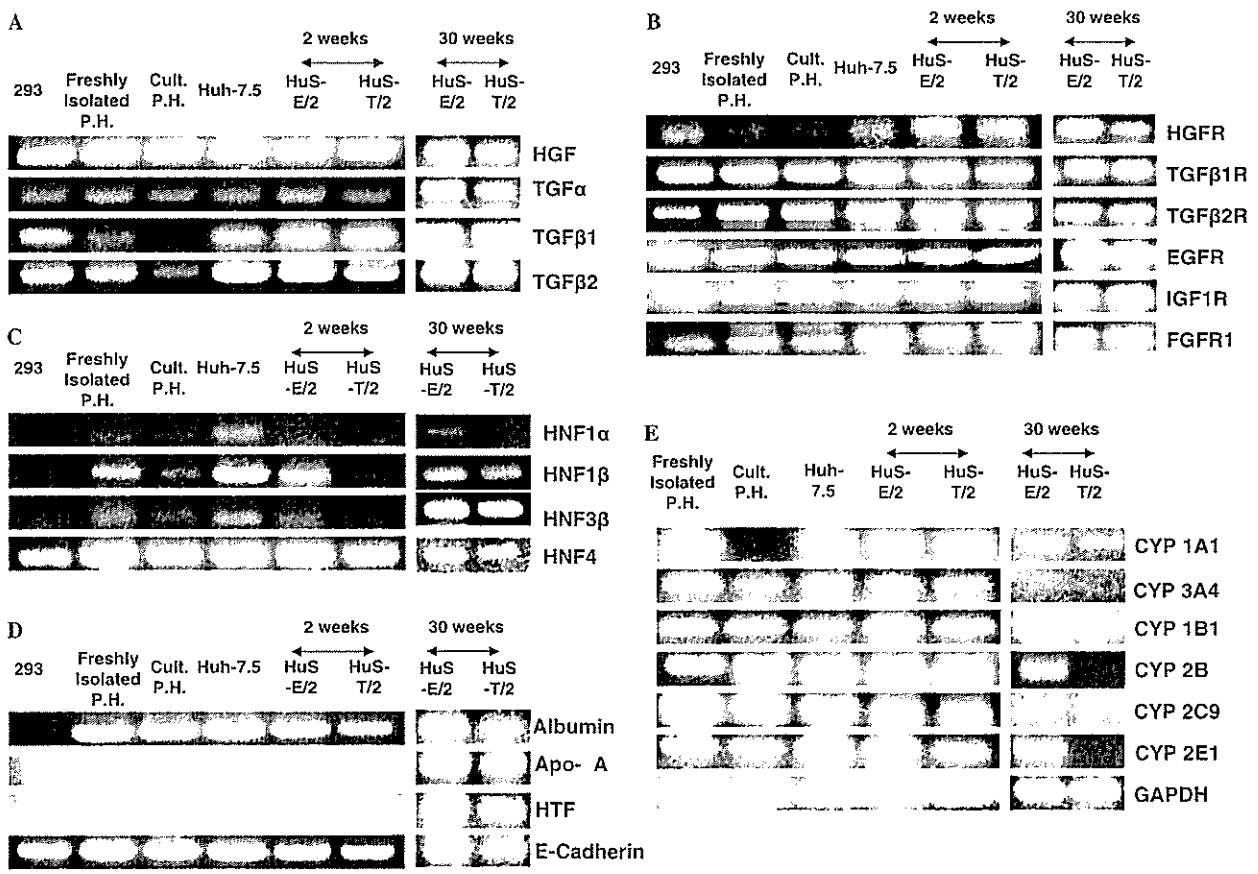

Fig. 2. Expression of the genes encoding growth factors (A), growth factor receptors (B), hepatocyte-specific nuclear factors (C), hepatocyte differentiation and functional markers (D), and CYP enzymes (E) in 293 cells, freshly isolated primary hepatocytes (P.H.), primary hepatocytes cultured for two weeks (Cult. P.H.), Huh-7.5 cells, and HuS-E/2 and HuS-T/2 cells cultured for two and 30 weeks were investigated by RT-PCR. The bands representing specific targets are indicated in the representative reactions.

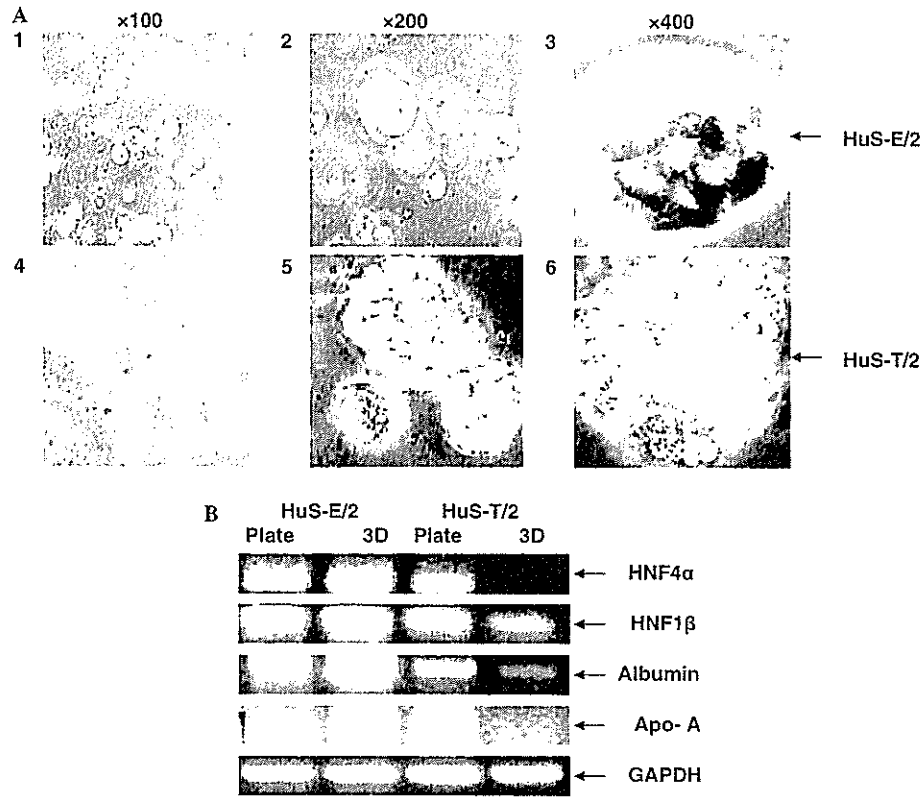

Fig. 3. (A) The morphology of HuS-E/2 and HuS-T/2 cells in 3D culture. HuSE/2 and HuS-T/2 cells were cultured in Mebiol Gel in 12-well plates at a concentration of 5×10^5 cells/well. The microscopic characteristics of these cells after one week of 3D culture are shown. (B) The expressions of HNF4α, HNF1β, albumin, and apo-A by HuS-E/2 and HuS-T/2 cells in both flat and 3D cultures are detailed. After one week of culture of HuS-E/2 and HuS-T/2 cells in flat and 3D cultures, the expressions of HNF4α, HNF1β, albumin, and apo-A were measured by RT-PCR in 250 ng total RNA.

HuS-T/2 but not in HuS-E/2 cells showed a transformed-like character starting from the 13th week of culture. This was demonstrated by continuing proliferation after confluence, pile-up formations (Fig. 1C), and proliferating in serum-deprevied condition. However, HuS-E/2 cells did not show any transformed-like characters even after 30 weeks of culture.

3.3. The characteristics of HuS-E and HuS-T immortalized hepatocytes in 3D culture

After one week in 3D culture, HuS-E/2 (Fig. 3A, panels 1, 2, and 3) cells adopted a donut-shaped structure with a central pore, while HuS-T/2 cells (Fig. 3A, panels 4, 5, and 6) displayed irregular mass formations (similar to the growth pattern of Huh-7.5 cells in 3D culture (data not shown)). In 3D culture, while the expression of HNF4, HNF1β, and albumin was enhanced in HuS-E/2, it was decreased in HuS-T/2 cells (Fig. 3B).

3.4. HCV infection to HuS-E/2

We further assessed the HCV infectivity of HuS-E- and HuS-T-derived clones by infection with HCV-1b-infected serum. Of the three HuS-E clones examined, HuS-E/2 clone demonstrated the highest infectability with HCV genotype 1b in comparison to Huh-7.5, PH5CH8 (Fig. 4A), and HuS-T cells (data not shown), which were excluded from further experiments.

3.5. Anti-CD81 blocked HCV infectivity

CD81 is involved in the entry of HCV pseudoparticles [24] and in vitro-synthesized JFH-1 [7]. To determine if authentic viral particles follow the same route of entry when infecting HuS-E/2 cells, we first examined the CD81 expression by RT-PCR. Both HuS-E/2 and HuS-T/2 cells expressed similar amounts of CD81 as freshly isolated hepatocytes and Huh-7.5 cells (Fig. 4B). Antibodies against CD81 reduced HCV infectivity of HuS-E/2 cells from the levels seen using a non-specific control antibody, confirming the importance of CD81 in HCV infectivity (Fig. 4C).

3.6. IFNα blocked HCV infectivity

We treated HuS-E/2 cells with HCV-containing serum. Cells were then cultured in fresh medium supplemented

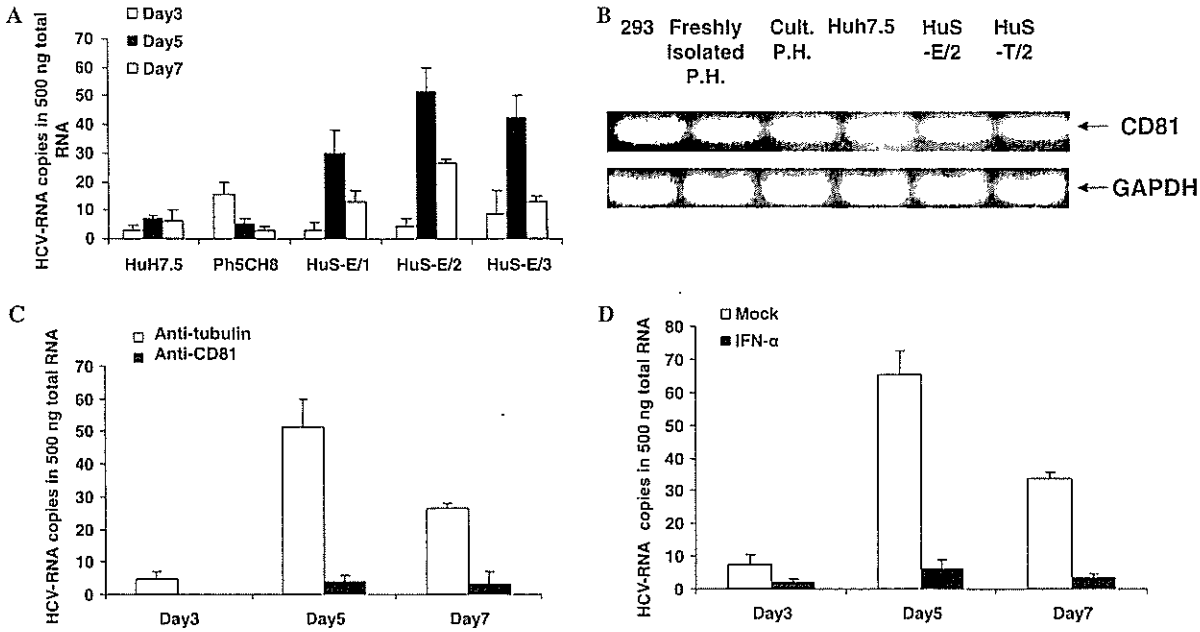

Fig. 4. (A) Serum from an HCV patient was used to infect Huh-7.5 cells, PH5CH8 cells, and three HPV E6E7-immortalized clones (HuS-E/1-3) for 24 h. After washing three times in phosphate-buffered saline (PBS), cells were cultured in fresh medium. Cells were then harvested and lysed at the indicated time points. The quantity of HCV genome RNA per 500 ng total RNA was determined by real-time RT-PCR analysis. (B) HuS-E/2 and HuS-T/2 cells both expressed CD81. Expression of CD81 (upper panel) and GAPDH as an internal control (lower panel) in 293 cells, freshly isolated P.H., cultured P.H., and Huh-7.5, HuS-E/2, and HuS-T/2 cells was investigated by RT-PCR. (C) Anti-CD81 antibodies blocked HCV infectivity. HCV infection was performed as described in (A) with the addition of CD81-specific (black bar) or anti-tubulin antibodies (control, white bar). (D) IFNα inhibits HCV multiplication in HuS-E/2 cells infected with HCV-containing serum. HuS-E/2 cells were infected with HCV as described in (A). After washing three times with PBS, cells were cultured in fresh medium supplemented with (black bar) or without (white bar) 100 U/ml IFNα.

without or with 100 U/ml IFNα. The enhancement of the HCV-RNA genome titers on the fifth day (about 10-fold) was not observed in cells treated continuously with IFNα (Fig. 4D). This result suggests that IFNα inhibited HCV replication in infected HuS-E/2 cells.

3.7. The effect of blocking IRF-3 and IRF-7 signaling on HCV infectivity

Production of interferon-alpha (IFNα) and interferon-beta (IFNβ) limits viral replication and spread, providing one of the most effective innate antiviral responses [25]. Signaling through IRF-3 and IRF-7 plays important roles in the stimulation of IFN-α/β production [25]. To determined which molecules (IRF-3 or IRF-7) play an important role in modulation of the innate immune response against HCV infection in these cells, we first detected intrinsic expression of double-stranded RNA-stimulated Toll-like receptor (TLR) 3, the downstream effector IRF-3, single-stranded RNA-stimulated TLR7, and 8, and the downstream effectors MyD88 and IRF-7 by RT-PCR. TLR3 exhibited very low expression in freshly isolated hepatocytes, Huh-7.5, HuS-E/2, and HuS-T/2 cells, while TLR7, TLR8, MyD88, and IRF-7 were easily detectable in both freshly isolated and immortalized cell lines (Fig. 5A).

The abilities of DNIRF-3 and DNIRF-7 to inhibit IFNβ and IFNα production by HuS-E/2 cells infected with Sendai virus were confirmed using assays of IFNβ or IFNα promoter-driven luciferase reporters. DNIRF-3 exhibited strong inhibition of IFNβ production (Fig. 5B) and weaker inhibition of IFNα transcription (Fig. 5C), while DNIRF-7 strongly inhibited IFNα production (Fig. 5C) and only weakly inhibited IFNβ production (Fig. 5B).

We then assessed the inhibition of HCV infectivity by DNIRF-3 and DNIRF-7. Transient transfection with DNIRF-3, DNIRF-7, or an empty vector was performed prior to HCV infection. Using Effectene reagent, the efficiency of plasmid transfection into HuS-E/2 cells was approximately 70% (data not shown). While there was no significant effect of DNIRF-3 on HCV infectivity, DNIRF-7 demonstrated a marked increase in HCV titers on days 3 and 5 after infection in comparison to control cells (Fig. 5D). To confirm that the enhancement of HCV replication by DNIRF-7 is not mediated by the impairment of IRF-3 signaling by heterodimeric interactions between IRF-3 and DNIRF-7, we performed siRNA inhibition of IRF-3 and IRF-7. The reduction of IRF-3 and IRF-7 expression by siRNA was obvious by RT-PCR (Fig. 5E). siRNA-mediated suppression of either IRF-3 or IRF-7 inhibited IFNβ and IFNα production

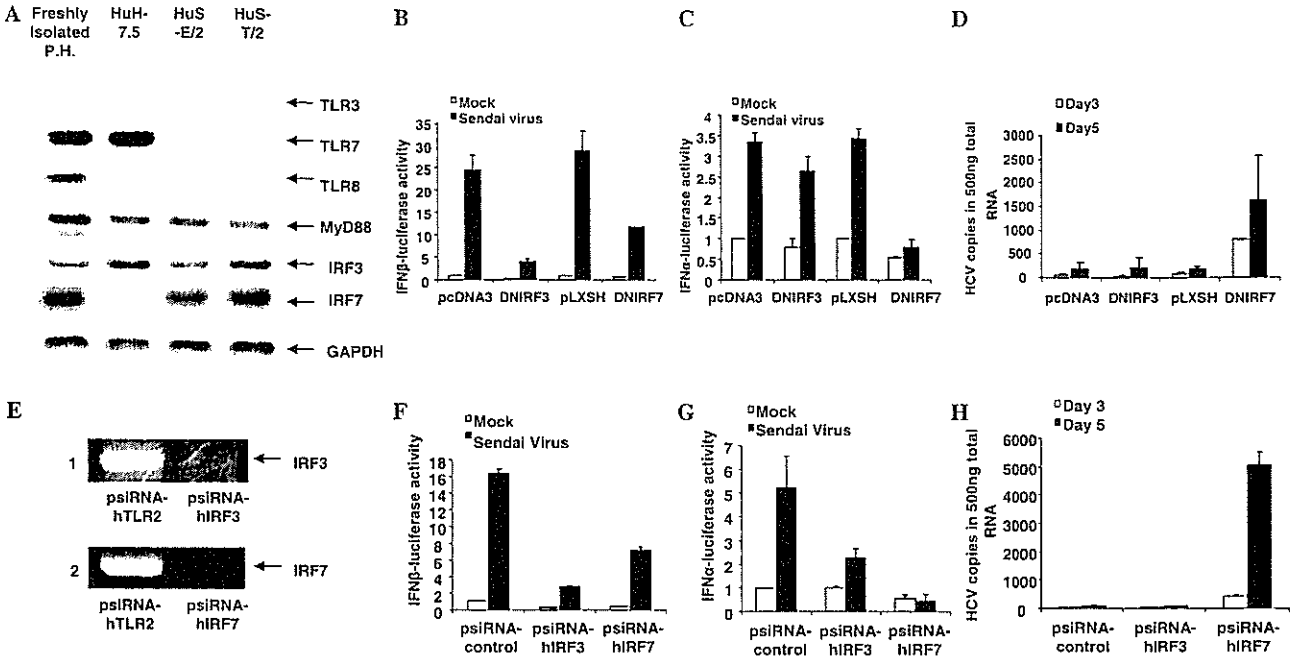

Fig. 5. (A) We examined the expression of TLR3, TLR7, TLR8, MyD88, IRF-3, and IRF-7, as well as GAPDH as an internal control in freshly isolated primary hepatocytes and Huh-7.5, HuS-E/2, and HuS-T/2 cells was investigated by RT-PCR. (B and C) HuS-E/2 cells were cotransfected with pIFNβ-luc (B) or pIFNα-luc (C) with an expression plasmid encoding DNIRF-3, DNIRF-7, or the appropriate empty vector (pcDNA3 and PLXSH, respectively). Twenty-four hours later, cells were infected (black bar) with Sendai virus or mock-infected (white bar), then analyzed for luciferase activity after 12 h. (D) IRF-7, but not IRF-3, suppression enhanced HCV infectivity of HuS-E/2 cells. HuS-E/2 cells were transiently transfected with empty pcDNA3, DNIRF-3, empty pLXSH, or DNIRF-7 plasmids. Twenty-four hours later, serum from a patient with HCV was used to infect transfected cells for 24 h. After washing, cells were cultured in fresh medium. The cells were then harvested and lysed at the indicated time points. The quantity of HCV genome RNA per 500 ng total RNA was determined by real-time RT-PCR analysis. (E) IRF-3 and IRF-7 levels were suppressed by specific siRNAs. HuS-E/2 cells were transfected with control psiRNA-hTLR2, psiRNA-hIRF-3, or psiRNA-hIRF-7, then selected with Zeocin at 250 μg/ml. Two weeks later, cells were harvested and assessed for the expression of IRF-3 and IRF-7 by RT-PCR. (F and G) HuS-E/2 cells were transfected with control psiRNA-hTLR2, psiRNA-hIRF-3, or psiRNA-hIRF-7, followed by selection in Zeocin at 250 μg/ml. Two weeks later, cells were cotransfected with pIFNβ-luc (F) or pIFNα-luc (G). Twenty-four hours later, cells were infected (black bar) with Sendai virus or mock-infected (white bar), then analyzed for luciferase activity after 12 h. (H) Transfected cells were infected with serum from HCV patient; HCV infectivity was assessed as described above.

in HuS-E/2 cells infected with Sendai virus in patterns similar to the effects seen following DNIRF-3 and DNIRF-7 expression, respectively (Figs. 5F and G). Blockade of IRF-7 expression resulted in a significantly higher titer of HCV after infection, while IRF-3 down-regulation did not have any significant effect on HCV titers (Fig. 5H). The enhancement of IRF-7 silencing by siRNA improved the infectivity of HCV (data not shown). These results suggest that IRF-7 plays the major role in the innate immune response to HCV in HuS-E/2 cells.

3.8. Establishment of stable DNIRF-7 expressing clones derived from HuS-E/2 cells

Since DNIRF-7 enhanced HCV infectivity, we transduced the plasmid encoding DNIRF-7 and a hygromycin-B resistance gene, into HuS-E/2 cells. Following selection with hygromycin-B, we obtained the HuS-E7/DN22 and HuS-E7/DN24 clones. As detected by RT-PCR, both clones demonstrated similar expression levels of albumin, apolipoprotein-A1, and HNF4 as the parental HuS-E/2 cells (Fig. 6A). The HuS-E7/DN24 clone exhibited stronger expression of DNIRF-7 than the HuS-E7/DN22 clone by immunoblotting (Fig. 6B). The induction of IFNα in HuS-E7/DN24 in response to infection with an RNA virus (Sendai virus) was low in comparison to the parental HuS-E/2 and HuS-E7/DN22 clones, as detected by IFNα-luciferase reporter assay (Fig. 6C). HuS-E7/DN24 also exhibited a higher HCV infectability in comparison to parental HuS-E/2 cells and the HuS-E7/DN22 clone (Fig. 6D).

3.9. Infection of HuS-E7/DN24 cells with different HCV genotypes

Huh7.5 and HuS-E7/DN24 cells were separately infected with serums derived from 3 different HCV-patients or by JFH-1 concentrated medium (HCV-2a). Two serums were infected by HCV-1b, while the third by HCV-2b. Inoculated virus titer was adjusted to be the same in all cases. Except for JFH-1, which efficiently

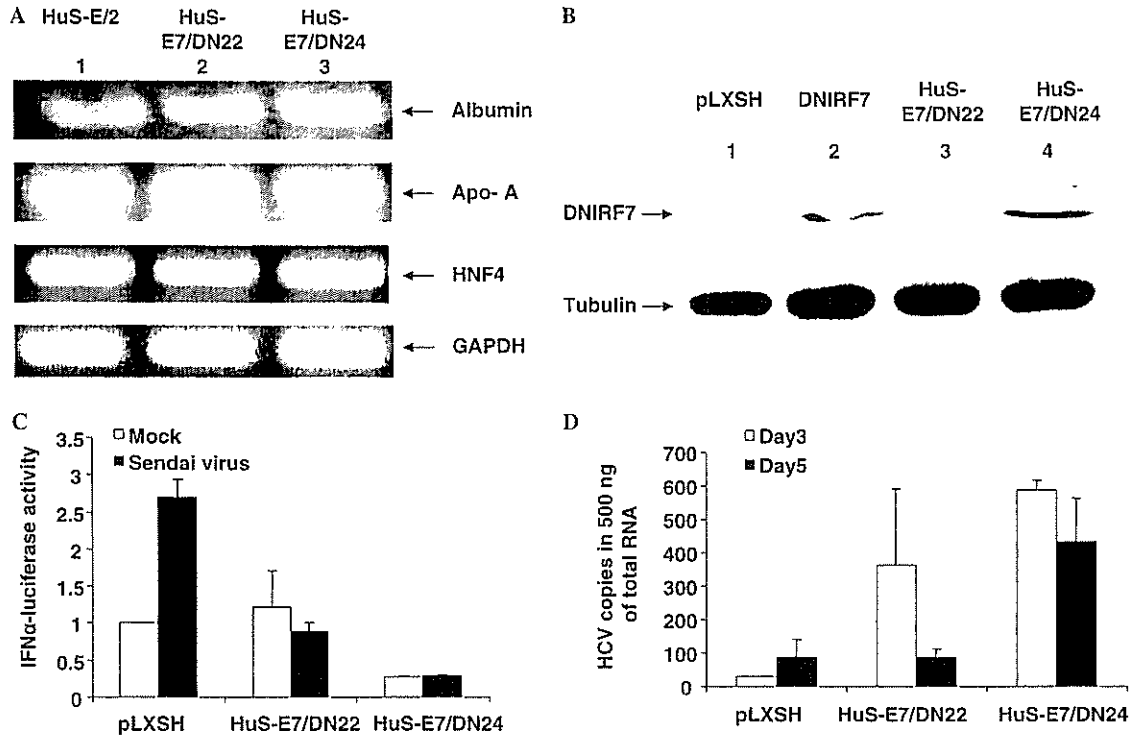

Fig. 6. (A) The pLXSH-HA-DNIRF-7 plasmid was transfected into HuS-E/2 cells, followed by selection in 100 μg/ml Hygromycin B. Two clones, HuS-E7/DN22 (lane 2) and HuS-E7/DN24 (lane 3), were obtained. We investigated the expression of albumin, apo-A, HNF4, and GAPDH as an internal control in parental HuS-E/2, HuS-E7/DN22, and HuS-E7/DN24 hepatocytes cultured for two weeks by RT-PCR. (B) Expression of HA-tagged DNIRF-7 (upper panel) and tubulin (control, lower panel) was detected by immunoblotting analysis. HuS-E/2 cells transiently transfected with either empty pLXSH vector (lane 1) or pLXSH-HA-DNIRF-7 (lane 2) were used as negative and positive controls, respectively, after 48 h. (C) HuS-E/2, HuS-E7/DN24, and HuS-E7/DN22 cells were transfected with IFNα-luc. HuS-E/2 cells were also cotransfected with pLXSH. All of these cells were then infected (black bar) or with Sendai virus or mock-infected, then analyzed for luciferase activity after 12 h. (D) HuS-E7/DN24 cells exhibited high infectivity to HCV samples derived from patient serum. HuS-E/2 cells were transiently transfected with empty pLXSH. Twenty-four hours later, serum from a recurrently transplanted HCV patient was used to infect transfected cells and HuS-E7/DN22 and HuS-E7/DN24 cells for 24 h. After washing three times, cells were cultured in fresh medium. Cells were then harvested and lysed at the indicated time points.

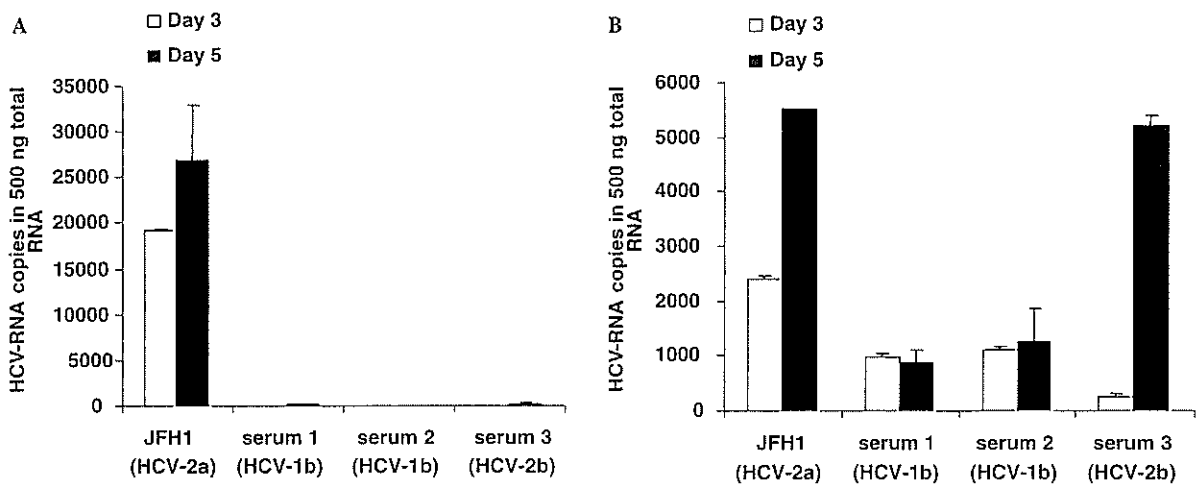

Fig. 7. The infectability of Huh-7.5 and HuS-E7/DN24 cells to different HCV genotypes. Huh-7.5 (A) and HuS-E7/DN24 (B) cells were infected with same titer of JFH1 (HCV-2a), two different HCV-1b serums and one HCV-2b serum. After removing the infected medium, the cells were washed in PBS and recultured in fresh medium. Cells were harvested and lysed at the indicated time points. The quantity of HCV genome RNA per 500 ng RNA was detected by real-time RT-PCR analysis.

replicated in Huh7.5 cells (Fig. 7A), HuS-E7/DN24 cells showed a higher and reproducible infectability for the different HCV strains than Huh7.5 cells (Fig. 7B). Similar higher infectability of HuS-E7/DN24 cells was observed with HCV-4a genotype (unpublished data). These results suggest that the high infectability of Huh-7.5 with JFH-1 is specific among the combinations of HCV strains and cell lines; while HuS-E7/DN24 cells were generally permissive to HCV-infected serum independent of HCV strains.

4. Discussion

This study demonstrates that ectopic expression of the HPV18/E6E7 genes in combination with hTERT could efficiently immortalize mature human hepatocytes, generating a cell line with stable expression of hepatocyte markers and functions for more than 30 weeks in culture. HuS-E/2 cells continuously exhibited higher expression of both HGF and HGFR than HuS-T/2 cells. This result suggests that HPV18/E6E7-immortalized hepatocytes maintain responsiveness to paracrine signals capable of inducing cell differentiation to a greater extent than SV40 T-immortalized hepatocytes. This conclusion is further supported by the increased expression of HNF4 in HuS-E/2 cells in comparison to HuS-T/2 cells. HNF4 is a major hepatocyte transcription factor, required for hepatocyte differentiation and liver-specific gene expression [26]. HNF4 drives hepatocytes differentiation by acting upstream in a transcription factor cascade that included HNF1α [27]. HuS-E/2 cells continued to express HNF1α throughout prolonged culture, while HuS-T/2 cells lost expression completely. Maintenance of hepatocellular functions was demonstrated by continuous and high expression of albumin, apolipoprotein-A, human transferrin, and E-cadherin by HuS-E/2 in comparison to HuS-T/2 cells. These differences became more pronounced in the late passages. In a similar manner, HuS-E/2 cells continued to express all of the examined CYP genes, with the exception of CYP 3A4, while HuS-T/2 cells lost expression of CYP 3A4, 1B, and 2E1 completely and displayed markedly lower expression of CYP 1B1 than HuS-E/2 cells. Thus, human hepatocytes immortalized by HPV E6/E7 transfection are phenotypically similar to primary hepatocytes, even during extended cultures.

Recently, it was reported that the JFH-1 strain and derived chimeras could only infect and propagate efficiently in Huh7.5.1 and Huh7.5 cells, both of which are subclones of Huh7 cells [7–9]. This limitation, however, may be specific to the JFH-1 **strain**, which may not accurately reflect the course of other HCV strains' infection. Thus, usage of HCV particles isolated from patient serum could be more useful to study authentic HCV infection. Using sera from HCV patients as a source of infective virus, HPV18/E6E7-immortalized cell lines exhibited higher reproducible susceptibility to HCV infection than HuS-T, PH5CH8, and Huh-7.5 cell lines.

IRF3 and IRF7 play an important role in the activation of interferon signaling [28]. We suppressed the functions of IRF-3 or IRF-7 to assess their role in HCV infectivity. In fact, we observed significant increase of HCV replication in HuS-E/2 cells bearing dominant-negative IRF7 that impaired IFN signaling. The suppression of IRF-3, however, did not have any significant effect on HCV infectivity or replication in this cell line. This may result from the blockade of IRF-3 activation by an HCV NS3/4A serine protease [29] through at least two independent pathways that inhibit the TLR3-dependent and RIG-I-dependent signaling pathways [29–33]. Although HCV was shown to inhibit basal expression levels of IRF-7 at both mRNA and protein levels and it was shown that NS5A suppresses IRF-7-induced IFNα promoter activation [34], Stimulation of TLR7 was shown to activate IRF-7 and induce suppression of HCV replicon levels in Huh-7 cells [35]. This suggests that the inhibition of IRF7 by HCV is not complete. Using IRF-7-deficient (IRF-7−/−) mice, Honda [36] demonstrated that the transcription factor IRF-7 is essential for the induction of IFNα/β genes. We established a clone stably expressing DNIRF-7 (HuS-7E/DN24), which demonstrated higher infectivity with different HCV strains than the parental HuS-E/2 clone.

In summary, we have established a human hepatocyte-derived cell line that maintains the characteristic features of primary hepatocytes by transduction with HPV18/E6E7. This cell line is highly infectable by HCV, which suggests that these cells may be useful to characterize the molecular mechanisms involved with HCV infection and to develop novel HCV treatment modalities.

Acknowledgements

We thank Dr. Akagi at Osaka Bioscience Institute for providing hTERT expressing vector, Dr. Sakai at the Institute for Virus Research, Kyoto University, for providing HPV18/E6E7 expressing plasmid, and Dr. Taniguchi of the University of Tokyo for providing IFNβ, and IFNα promoters' reporter plasmids. This work was supported by Grants-in-Aid for cancer research and for the second-term comprehensive 10-year strategies for cancer control from the Ministry of Health, Labor and Welfare, by Grants-in-Aid for scientific research from the Ministry of Education, Culture, Sports, Science and Technology, by Grants-in-Aid for the research for the future program from the Japanese society for the Promotion of Science. Dr. Hussein H. Aly is a receiver of the Japanese *Gakushu Shoreihi* scholarship and was partly supported by Prof. *Yassin A. El Ghaffar memorial scholarship* for the Improvement of Liver research in Egypt.

References

[1] Wasley A, Alter MJ. Epidemiology of hepatitis C: geographic differences and temporal trends. Semin Liver Dis 2000;20:1–16.

[2] Manns MP, McHutchison JG, Gordon SC, Rustgi VK, Shiffman M, Reindollar R, et al. Peginterferon alfa-2b plus ribavirin compared with interferon alfa-2b plus ribavirin for initial treatment of chronic hepatitis C: a randomised trial. Lancet 2001;358:958–965.

[3] Fried MW, Shiffman ML, Reddy KR, Smith C, Marinos G, Goncales Jr FL, et al. Peginterferon alfa-2a plus ribavirin for chronic hepatitis C virus infection. N Engl J Med 2002;347: 975–982.

[4] Hadziyannis SJ, Sette Jr H, Morgan TR, Balan V, Diago M, Marcellin P, et al. Peginterferon-alpha2a and ribavirin combination therapy in chronic hepatitis C: a randomized study of treatment duration and ribavirin dose. Ann Intern Med 2004;140:346–355.

[5] Muir AJ, Bornstein JD, Killenberg PG. Peginterferon alfa-2b and ribavirin for the treatment of chronic hepatitis C in blacks and non-Hispanic whites. N Engl J Med 2004;350:2265–2271.

[6] Falck-Ytter Y, Kale H, Mullen KD, Sarbah SA, Sorescu L, McCullough AJ. Surprisingly small effect of antiviral treatment in patients with hepatitis C. Ann Intern Med 2002;136:288–292.

[7] Wakita T, Pietschmann T, Kato T, Date T, Miyamoto M, Zhao Z, et al. Production of infectious hepatitis C virus in tissue culture from a cloned viral genome. Nat Med 2005;11:791–796.

[8] Zhong J, Gastaminza P, Cheng G, Kapadia S, Kato T, Burton DR, et al. Robust hepatitis C virus infection in vitro. Proc Natl Acad Sci USA 2005;102:9294–9299.

[9] Lindenbach BD, Evans MJ, Syder AJ, Wolk B, Tellinghuisen TL, Liu CC, et al. Complete replication of hepatitis C virus in cell culture. Science 2005;309:623–626.

[10] Dellgado JP, Parouchev A, Allain JE, Pennarun G, Gauthier LR, Dutrillaux AM, et al. Long-term controlled immortalization of a primate hepatic progenitor cell line after Simian virus 40 T-Antigen gene transfer. Oncogene 2005;24:541–551.

[11] Mizuguchi T, Mitaka T, Katsuramaki T, Hirata K. Hepatocyte transplantation for total liver repopulation. J Hepatobiliary Pancreat Surg 2005;12:378–385.

[12] Isom HC, Tevethia MJ, Kreider JW. Tumorigenicity of simian virus 40-transformed rat hepatocytes. Cancer Res 1981;41: 2126–2134.

[13] Ray FA, Waltman MJ, Lehman JM, Little JB, Nickoloff JA, Kraemer PM. Identification of SV40 T-antigen mutants that alter T-antigen-induced chromosome damage in human fibroblasts. Cytometry 1998;31:242–250.

[14] Chen WH, Lai WF, Deng WP, Yang WK, Lo WC, Wu CC, et al. Tissue engineered cartilage using human articular chondrocytes immortalized by HPV-16 E6 and E7 genes. J Biomed Mater Res A 2006;76:512–520.

[15] Dimri G, Band H, Band V Mammary epithelial cell transformation: insights from cell culture and mouse models. Breast Cancer Res 2005;7:171–179.

[16] Harms W, Rothamel T, Miller K, Harste G, Grassmann M, Heim A. Characterization of human myocardial fibroblasts immortalized by HPV16 E6–E7 genes. Exp Cell Res 2001;268:252–261.

[17] Shiga T, Shirasawa H, Shimizu K, Dezawa M, Masuda Y, Simizu B. Normal human fibroblasts immortalized by introduction of human papillomavirus type 16 (HPV-16) E6-E7 genes. Microbiol Immunol 1997;41:313–319.

[18] Akimov SS, Ramezani A, Hawley TS, Hawley RG. Bypass of senescence, immortalization, and transformation of human hematopoietic progenitor cells. Stem Cells 2005;23:1423–1433.

[19] Hung SC, Yang DM, Chang CF, Lin RJ, Wang JS, Low-Tone Ho L, et al. Immortalization without neoplastic transformation of human mesenchymal stem cells by transduction with HPV16 E6E7 genes. Int J Cancer 2004;110:313–319.

[20] Wang G, Johnson GA, Spencer TE, Bazer FW. Isolation, immortalization, and initial characterization of uterine cell lines: an in vitro model system for the porcine uterus. In vitro Cell Dev Biol Anim 2000;36:650–656.

[21] Hino H, Tateno C, Sato H, Yamasaki C, Katayama S, Kohashi T, et al. A long-term culture of human hepatocytes which show a high growth potential and express their differentiated phenotypes. Biochem Biophys Res Commun 1999;256:184–191.

[22] Watashi K, Hijikata M, Hosaka M, Yamaji M, Shimotohno K. Cyclosporin A suppresses replication of hepatitis C virus genome in cultured hepatocytes. Hepatology 2003;38:1282–1288.

[23] Murata T, Ohshima T, Yamaji M, Hosaka M, Miyanari Y, Hijikata M, et al. Suppression of hepatitis C virus replicon by TGF-beta. Virology 2005;331:407–417.

[24] Dasgupta A, Hughey R, Lancin P, Larue L, Moghe PV. E-cadherin synergistically induces hepatospecific phenotype and maturation of embryonic stem cells in conjunction with hepatotrophic factors. Biotechnol Bioeng 2005;92:257–266.

[25] Civas A, Island ML, Genin P, Morin P, Navarro S. Regulation of virus-induced interferon-A genes. Biochimie 2002;84:643–654.

[26] Ishiyama T, Kano J, Minami Y, Iijima T, Morishita Y, Noguchi M. Expression of HNFs and C/EBP alpha is correlated with immunocytochemical differentiation of cell lines derived from human hepatocellular carcinomas, hepatoblastomas and immortalized hepatocytes. Cancer Sci 2003;94:757–763.

[27] Wege H, Le HT, Chui MS, Liu L, Wu J, Giri R, et al. Telomerase reconstitution immortalizes human fetal hepatocytes without disrupting their differentiation potential. Gastroenterology 2003;124: 432–444.

[28] Mamane Y, Heylbroeck C, Genin P, Algarte M, Servant MJ, LePage C, et al. Interferon regulatory factors: the next generation. Gene 1999;237:1–14.

[29] Foy E, Li K, Wang C, Sumpter Jr R, Ikeda M, Lemon SM, et al. Regulation of interferon regulatory factor-3 by the hepatitis C virus serine protease. Science 2003;300:1145–1148.

[30] Sumpter Jr R, Loo YM, Foy E, Li K, Yoneyama M, Fujita T, et al. Regulating intracellular antiviral defense and permissiveness to hepatitis C virus RNA replication through a cellular RNA helicase, RIG-I. J Virol 2005;79:2689–2699.

[31] Breiman A, Grandvaux N, Lin R, Ottone C, Akira S, Yoneyama M, et al. Inhibition of RIG-I-dependent signaling to the interferon pathway during hepatitis C virus expression and restoration of signaling by IKKepsilon. J Virol 2005;79:3969–3978.

[32] Li K, Foy E, Ferreon JC, Nakamura M, Ferreon AC, Ikeda M, et al. Immune evasion by hepatitis C virus NS3/4A protease-mediated cleavage of the Toll-like receptor 3 adaptor protein TRIF. Proc Natl Acad Sci USA 2005;102:2992–2997.

[33] Foy E, Li K, Sumpter Jr R, Loo YM, Johnson CL, Wang C, et al. Control of antiviral defenses through hepatitis C virus disruption of retinoic acid-inducible gene-I signaling. Proc Natl Acad Sci USA 2005;102:2986–2991.

[34] Zhang T, Lin RT, Li Y, Douglas SD, Maxcey C, Ho C, et al. Hepatitis C virus inhibits intracellular interferon alpha expression in human hepatic cell lines. Hepatology 2005;42:819–827.

[35] Lee J, Wu CC, Lee KJ, Chuang TH, Katakura K, Liu YT, et al. Activation of anti-hepatitis C virus responses via Toll-like receptor 7. Proc Natl Acad Sci USA 2006;103:1828–1833.

[36] Honda K, Yanai H, Negishi H, Asagiri M, Sato M, Mizutani T, et al. IRF-7 is the master regulator of type-I interferon-dependent immune responses. Nature 2005;434:772–777.

Available online at www.sciencedirect.com

ScienceDirect

Biochemical and Biophysical Research Communications 352 (2007) 170–176

BBRC

www.elsevier.com/locate/ybbrc

Helper virus-independent *trans*-replication of hepatitis C virus-derived minigenome

Jing Zhang [a,*], Osamu Yamada [a], Hiroshi Yoshida [a], Takashi Sakamoto [a], Hiromasa Araki [a], Kunitada Shimotohno [b]

[a] *Research and Development Center, FUSO Pharmaceutical Industries, LTD., 2-3-30 Morinomiya, Joto-ku, Osaka 536-8523, Japan*
[b] *Department of Viral Oncology, The Institute for Virus Research, Kyoto University, Kyoto 606-8397, Japan*

Received 25 October 2006
Available online 13 November 2006

Abstract

We have previously described a synthetic T7-driven cDNA minigenome containing the antisense sequence of luciferase gene and internal ribosome entry site of encephalomyocarditis virus flanked by 5′- and 3′-end sequences of hepatitis C virus (HCV) that contain *cis*-acting replication elements. Synthesis of minus-strand RNA from the artificial minigenome was determined by using Huh-7 cells harboring autonomously replicating HCV subgenome as a helper for provision of functional replication components. To further confirm and extend these studies, we investigated here whether the minigenome replication system could be reconstituted by transfection of naïve Huh-7 cells with plasmid expressing nonstructural (NS) proteins. Reporter assay and Northern blot analysis revealed that *trans*-expression of NS proteins from 3 to 5 resulted in high level of luciferase activity and synthesized minus-strand RNA. The analogous result was also obtained with the minigenome derived from HCV 2a, and both HCV 1b- and 2a-derived NS protein were able to support the chimeric minigenomes whose 5′- or 3′-end was replaced by the respective region of the heterologous virus. These results provide a basis for establishing the reverse genetic system that is helpful to study *cis*- and *trans*-acting factors involved in HCV RNA replication.

Keywords: Hepatitis C virus; Minigenome; *trans*-Replication

Hepatitis C virus (HCV) is an important human pathogen with an estimated 170 million chronic carriers throughout the world, and many of them are at a high risk for developing liver cirrhosis and hepatocellular carcinoma [1]. HCV is a member of the *Flaviviridae* family with a positive-sense RNA genome of ~9600 nucleotides in length. The genome is flanked by highly structured nontranslated regions (NTRs) important for both RNA translation and replication. The viral genome encodes a polyprotein precursor of approximately 3010 amino acids, which is processed by viral and cellular protease to produce the structural proteins (core, E1, and E2) and nonstructural (NS) proteins (p7 and NS2 to NS5B).

Like other plus-stranded RNA viruses, HCV genomic RNA is first transcribed into a minus-strand intermediate, which in turn serves as the template for production of progeny plus-strand RNA. Although the basic steps in replication have been well established, little is known about the detail of these processes. Studies of HCV replication have been hampered by the lack of an efficient tissue culture system. Although the development of subgenomic replicon has facilitated the investigation of viral RNA replication in cell culture [2], culture-adaptive mutations within the NS proteins are required for efficient replication [3,4], and full-length genomes carrying such mutations do not produce infectious virus particles [5,6]. More recently, it was reported that genotype 2a JFH1 genome replicates efficiently independent of the culture-adaptive mutations and supports production of viral particles [7]. This *in vitro* system, together with the later-developed JFH1-based

* Corresponding author. Fax: +81 6 6964 2706.
E-mail address: j-zhang@fuso-pharm.co.jp (J. Zhang).

0006-291X/$ - see front matter © 2006 Elsevier Inc. All rights reserved.
doi:10.1016/j.bbrc.2006.10.188

chimeras [8,9], are an important progress in HCV research, allowing the study of unknown aspects of HCV life cycle. However, a comparison study showed that JFH1 differs from the earlier-generated HCV 1b replicon in independence of the cellular cofactor (cyclophilin B) for the replication and less sensitivity to antiviral reagent [10], suggesting that the strain- or genotype-specific properties may exist and the observation obtained with JFH1 cannot be simply extrapolated to other isolates.

Synthetic minigenomes have been described in a number of minus- and plus-stranded RNA viruses, which has contributed greatly to the analysis of *cis*-acting sequences and *trans*-acting proteins required for viral replication, maturation, and packaging [11,12]. We previously established a helper virus-dependent expression system utilizing HCV-derived minigenome, and Huh-7 cells harboring autonomously replicating HCV subgenome [13]. In this study, we further investigated whether the minigenome replication system could be reconstituted by transfection of naïve Huh-7 cells with plasmid expressing NS proteins. It was shown that synthesis of minus-strand RNA from HCV minigenome can be supported by *trans*-expressed polyprotein NS3 to NS5B, and the NS proteins were able to replicate not only the homologous minigenome but the heterologous and chimeric minigenome as well.

Materials and methods

Plasmids. HCV 1b-derived minigenome p1b-1b was previously referred to as pT7cRLNS5B1 [13]. For construction of chimeric minigenome p2a-1b, the first 376 nucelotides of HCV 2a cDNA with the T7 promoter directly coupled at the 5′-end were amplified by PCR with primers 5′-tataa gcttTAATACGACTCACTATAACCTGCCCCTAATAGGGGC-3′ and 5′-tgcgcatgcTTTGGTTTTTCTTTGAGGTT-3′. The *Renilla* luciferase gene was amplified from pRL-TK (Promega) using primers 5′-ctctctagaA TGACTTCGAAAGTTTATGA-3′ and 5′- tgcgcatgcTTATTGTTCATT TTTGAGAA-3′. The resulting PCR products were digested with *Hin*dIII–*Sph*I and *Sph*I–*Xba*I, respectively, and inserted into the *Hin*dIII/*Xba*I sites of p1b-1b. The 3′- part of the NS5B coding region fused 3′ UTR of HCV 2a cDNA was amplified by PCR using primers 5′-ataggatccCCTCAGAA AACTTGGGG-3′ and 5′-ataggcgccagcgaggaggctgggaccatgccggccACAT GATCTGCAGAGAGACC-3′, digested with *Bam*HI and *Nar*I, and cloned, along with the annealed oligonucleotides containing partial sequence of the HDV ribozyme [13], into *Bam*HI/*Eco*RI-cut p1b-1b or p2a-1b, creating p1b-2a and p2a-2a, respectively.

To construct plasmid pNS3-51b expressing polyprotein from HCV 1b, a cDNA containing the ORF of NS3 to NS5B was amplified with primers 5′-atatctagaATGGGCCCATCACGGCTTA-3′ and 5′-ataggcgcgccTCA CCGGTTGGGGAGCAGG-3′, digested with *Xba*I and *Asc*I, and cloned, along with *Hin*dIII/*Xba*I-cut HCV sequence (1–341 nt), into pGEMEX-1 vector (Promega) which was modified by deletion of all of the T7 gene 10 and introduction of *Hin*dIII and *Asc*I sites between T7 promoter and terminator [14]. pNS3-52a, which expresses the polyprotein from HCV 2a, was constructed similarly except with the primers of corresponding sequence from genotype 2a. The sequences of these constructs were confirmed by nucleotide sequencing.

Cells. The cell line Huh-7 was purchased from the American Type Culture Collection (ATCC) and maintained in Dulbecco's modified Eagle's medium (DMEM, Invitrogen) supplemented with 10% fetal calf serum and 50 U/ml penicillin and streptomycin in a 5% CO_2 humidified atmosphere. A Huh-7-derived cell line (Huh–NNRZ) stably replicating HCV subgenomic replicon was grown in DMEM containing 300 μg/ml G418 (Geneticin, Invitrogen) [15,16].

Transfection. Huh-7 cells were seeded at 1×10^5 per well of 12-well plates. Twenty-four hours later, 0.5 μg *Eco*RI-linearized minigenome (p1b-1b, p1b-2a, p2a-1b, or p2a-2a), 0.5 μg pGEMEX-1, pNS3-51b, or pNS3-52a, 0.5 μg pAM8-1, and 0.1 μg pGL3-Control vector were cotransfected into cells with Fugene HD Transfection Reagent (Roche). The cells were harvested at the indicated time points, and cell lysates were assayed for luciferase activity as described below.

Luciferase assay. Cell lysates were prepared from transfected cells, centrifuged briefly, and 20 μl of the supernatants was used for luciferase assays with Dual-Luciferase Reporter Assay System (Promega) according to the manufacturer's instructions. Luciferase activities were measured using a TD-20/20 Luminometer (Promega).

Western blot analysis. Protein was electrophoresed on a sodium dodecyl sulfate–polyacrylamide gel, transferred to Hybond-P PVDV Membrane (Amersham). The blots were probed with Antiserum Product 2871 and 2881 (ViroStat) for detection of NS3 and NS4, rabbit polyclonal antibody (ab2594, Abcam Limited) for NS5A, and goat polyclonal antibody (sc-17532, Santa Cruz Biotechnology, Inc.) for NS5B. Signals were visualized with ECL Plus Western Blotting Detection Reagents (Amersham).

Northern blot analysis. RNAs were isolated from transfected cells with Trizol reagent (Invitrogen) and treated with RNase-free DNase (Promega). The purified RNAs were separated by denaturing agarose gel electrophoresis and analyzed by Northern blot using digoxigenin-labeled antisense *Renilla* luciferase sequence.

Results

Synthetic minigenome derived from HCV

The minigenome construct derived from HCV 1b consists of the antisense sequence of the *Renilla* luciferase gene and internal ribosome entry site (IRES) of encephalomyocarditis virus (EMCV) flanked upstream by 5′-end (nucleotides 1–377) and downstream by 3′-end sequence containing NS5B coding region from nucleotides 9067 to 9371 plus 3′-UTR of HCV cDNA. The cassette was positioned precisely at the T7 transcription start site followed by self-cleaving HDV ribozyme to ensure authentic 5′- and 3′-ends (Fig. 1A, p1b-1b). If the minigenome could be accepted as a template by the replication complex provided in *trans*, the luciferase gene, which is encoded by synthesized minus-strand RNA, would express in HCV-infected cells. Fully consistent with this hypothesis, luciferase activity was selectively detected in Huh-7 cells harboring an autonomously replicating HCV subgenome (Huh–NNRZ) [13].

Replication of HCV minigenome in Huh-7 cells expressing polyprotein NS3 to NS5B

The ability of the synthetic minigenome to replicate in replicon cells prompted us to investigate whether the replication of minigenome could be supported by HCV proteins expressed in *trans*. For this purpose, Huh-7 cells were transfected with the minigenomic construct p1b-1b, plasmid encoding a polyprotein encompassing NS3 to NS5B under the control of T7 RNA polymerase promoter, pAM8-1 plasmid expressing T7 RNA polymerase [14], and pGL3-Control vector. The cells were harvested at 3